

**A CASE STUDY OF THE INTERNAL STRUCTURES OF GOSSANS AND WEATHERING PROCESSES
IN THE IBERIAN PYRITE BELT USING MAGNETIC FABRICS AND PALEOMAGNETIC DATING**

Mourad Essalhi¹, Stanislas Sizaret^{1*}, Luc Barbanson¹, Yan Chen¹, France Lacroix², François Demory³, José M. Nieto⁴, Reinaldo Sáez⁴, M. Ángeles Capitán⁴

¹Université d'Orléans, CNRS/INSU, Institut des Sciences de la Terre d'Orléans - UMR 6113
Campus Géosciences 1A, rue de la Férellerie, 45071 Orléans cedex 2, France

²Laboratoire de Paléomagnétisme, Institut de physique du Globe de Paris, 4, Place de Jussieu,
75 252 Paris cedex 05, France.

³CEREGE, Université Aix Marseille—CNRS, Europôle de l'Arbois, BP 80 13545, Aix En
Provence, France

⁴Departamento de Geología, Universidad de Huelva, Av. Fuerzas Armadas s/n, 21071
Huelva, Spain

*Corresponding author: e-mail: stanislas.sizaret@univ-orleans.fr, Tel: +33 2 38 49 25 96, Fax:
+33 2 38 63 64 88

Abstract In the Rio Tinto district of the Iberian Pyrite Belt of South Spain, the weathering of massive sulphide bodies form iron caps, i.e. true gossans and their subsequent alteration and re-sedimentation has resulted in iron terraces, i.e. displaced gossans. To study the structure and evolution of both types of gossans, magnetic investigations have been carried out with two foci: (i) the characterisation and spatial distribution of magnetic fabrics in different mineralised settings, including massive sulphides, gossans and terraces, and (ii) paleomagnetic dating. Hematite has been identified as the susceptibility carrier in all sites and magnetic fabric investigation of four gossans reveals a vertical variation from top to

bottom, with: (i) a horizontal foliation referred to as “mature” fabric in the uppermost part of the primary gossans; (ii) highly inclined or vertical foliation interpreted as “immature” fabric between the uppermost and lowermost parts, and (iii) a vertical foliation interpreted to be inherited from Hercynian deformation in the lowermost part of the profiles. In terraces, a horizontal foliation dominates and is interpreted to be a “sedimentary” fabric. Rock magnetic studies of gossan samples have identified goethite as the magnetic remanence carrier for the low temperature component (LTC), showing either a single direction close to the present Earth field (PEF) direction or random directions. Maghemite, hematite and occasionally magnetite are the remanence carriers for the stable high temperature component (HTC) that is characterized by non PEF directions with both normal and reversed magnetic polarities. No reliable conclusion can be yet drawn on the timing of terrace magnetization due to the small number of samples. In gossans, the polarity is reversed in the upper part and normal in the lower part. This vertical distribution with a negative reversal test suggests remanence formation during two distinct periods. Remanence in the upper parts of the gossans is older than in the lower parts, indicating that the alteration proceeded from top to bottom of the profiles. In the upper part, the older age and the horizontal “mature” fabric is interpreted to be a high maturation stage of massive sulphides’ alteration. In the lower part, the age is younger and the inherited “immature” vertical Hercynian fabric indicates a weak maturation stage. These two distinct periods may reflect changes of paleoclimate, erosion and/or tectonic motion.

Keywords: AMS, Iberian Pyrite Belt, gossans, massive sulphides, terraces, magnetic fabric, paleomagnetic dating.

Introduction

Iron cap is an iron oxi-hydroxides-rich superficial material formed by oxidation, weathering or decomposition of former rocks. In metallogeny, a gossan is an iron cap formed by intensive weathering and oxidation of sulphides that is located on the upper part of sulphide mineralization (Kosakevitch 1979; Wilhelm and Kosakevitch 1978; 1979). A classic gossan is composed mainly of neoformed iron oxi-hydroxides with residual unaltered minerals such as quartz. In addition to manganese and iron oxi-hydroxides, various precious metals and minerals, such as gold and silver and various sulfate and silicate minerals can occur in gossans. Commonly, gossans appear as a red stain to the country rocks and soil due to the abundance of oxidized iron and they may form elevated plateaus due to the abundance of erosion-resistant quartz and iron oxides. Gossans are considered also to be an important marker for the exploration of ore deposits (Kosakevitch 1979; Wilhelm and Kosakevitch 1978; Assiri and Moussa 2008). Previous studies on gossans are focused mostly on the geochemistry, environmental impacts and life in extreme environments (*e.g.* Boyle 1995; Scott et al. 2001; Al et al. 2006; Egal 2008). Studies of gossan formation and evolution are less common. Moreover, paleomagnetic studies to date gossan formation, such as the Murray Brook and Heath Steele Au-Ag gossan deposits are rare (Symons et al. 1996), and to our knowledge, no investigation on magnetic fabrics of a gossan has ever been performed. However, these fabrics and their associated sulphides may help to understand the processes involved in gossan formation. Anisotropy of Magnetic Susceptibility (AMS) is the principal technique used in this work. AMS has proven to be an efficient technique to quantify the preferred orientation of magnetic fabrics with a high sensitivity and therefore is considered to be a powerful tool to study the texture of rocks (*e.g.* Rochette et al. 1992; Tarling and Hrouda

1993; Sizaret et al. 2003). AMS has been applied in fields such as structural geology and rock petrofabrics (*e.g.* Hrouda 1982; Tarling and Hrouda 1993), granitic pluton emplacement (*e.g.* Jover et al. 1989; Bouillin et al. 1993; Talbot et al. 2005), magmatic flow direction (*e.g.* Nomade et al. 2000), rock deformation (*e.g.* Borradaile and Tarling 1981; Evans et al. 2003), and recently to track paleoflow circulation (*e.g.* Sizaret et al. 2001; Sizaret et al. 2006a and b; Essalhi et al. 2009; Sizaret et al. 2009). Although the AMS method has already been applied to weathered soils (*e.g.* Le Borgne 1955; Özdemir and Banerjee 1982) and lateritic profiles (*Cf.* Mathé et al. 1999; Théveniaut and Freyssinet 1999), no AMS study has been devoted so far to gossans.

Actively explored since the Chalcolithic era, the Iberian Pyrite Belt (IPB) is one of the world's oldest and most important sulphide mining districts with original reserves estimated at > 1700 Mt (Sáez et al. 1996) and a mining history of > 4500 years (Leblanc et al. 2000; Sáez et al. 2003). These deposits are located in an arc-shaped belt of \approx 230 km in length and \approx 40 km in width, extending from Seville in Spain to south of Lisbon in Portugal. Several structural, petrological and geochemical studies have been published on the IPB (*e.g.* Leistel et al. 1998; Sáez et al. 1999). The sulphide deposits were formed during the Devonian-Carboniferous period and folded by the Variscan orogeny. Percolation of meteoritic water within the massive sulphides and associated stockworks induced the formation of gossans above the water table.

The process of gossan formation starts with the oxidation of pyrite and other sulphides to form Fe oxy-hydroxides plus sulfuric acid. The initial product of weathering is typically an amorphous ferric hydroxide expressed as $\text{Fe}(\text{OH})_3$ that gradually crystallizes to goethite and/or hematite. Other important associated minerals with the Fe oxy-hydroxides are jarosite, gypsum, clay minerals and silica (*e.g.* Atapour and Aftabi 2007).

The aim of the present study is to describe the magnetic fabric and to date terrace and gossan formation, in order to better understand the sulphide weathering processes in the Spanish part of the Iberian Pyrite Belt.

Geological setting of the Iberian Pyrite Belt

The IPB with the Baja–Acebuches ophiolitic complex and Pulo do Lobo antiform constitute the South Portuguese Zone (Fig. 1a). The IPB stratigraphic succession is composed of three main units that rest on an unknown substratum (Figs. 1a and 1b). The lowest unit is the Late Devonian Phyllite–Quartzite (PQ) formation, which is about 1000 to 5000 m thick and composed mainly of alternating sandstone and shale. This formation is characterized by typical stable epicontinental platform features (Moreno et al. 1996). The boundary between the PQ formation and the intermediate unit is defined by quartz–arenite layers (Moreno et al. 1996). The middle unit is the Late Famennian to Late Visean Volcano-Sedimentary Complex (VSC; Van den Boogaard 1963; Oliveira 1990) that is composed of three acidic volcanic cycles separated by two basic volcanic cycles (Lécolle 1972; Routhier et al. 1980) with mudstone and some chemical sediments. The VSC varies in thickness between 100 and 1300 m. The IPB massive sulphide deposits are hosted in the VSC. The youngest unit in the IPB is the Culm Group (Moreno, 1993), which ranges from Late Visean to Middle-Late Pennsylvanian (Oliveira 1990). The Culm group is a detrital unit of synorogenic turbidites up to 3000 m thick. The whole succession of the IPB suffered slight regional metamorphism during the Hercynian Orogeny (Munhá 1979, 1990; Abad et al. 2001). Deformation in the IPB has been extensively discussed and a thin-skinned tectonic model is widely accepted that describes the IPB as a southward-verging thrust and fold belt (Schermerhorn and Stanton

1969; Schermerhorn 1971; Ribeiro and Silva 1983; Silva et al. 1990; Soriano 1996; Quesada 1998; Onézime et al. 2002).

Massive sulphide metallogeny in the IPB

Three sulphide deposit styles coexist in the IPB: massive ore bodies, stockworks and disseminations. Devonian-Carboniferous mineralization took place during the Variscan orogeny at about 350 Ma (Re-Os isotopic method; Mathur et al. 1999; Nieto et al., 1999). Palynology has provided a similar age in several sectors of the IPB, such as Tharsis, Aznalcóllar, Sotiel-Coronada or Neves-Corvo (González et al. 2002; Sáez et al. 2008), which suggest that a single mineralization event was responsible for the genesis of all massive sulphide deposits in the IPB.

The massive sulphides of the IPB are associated with volcanic (Río Tinto), volcanoclastic (La Zarza) or purely sedimentary rocks (Tharsis). These massive sulphides constitute an intermediate genetic type between the Clastic-dominated sediment hosted and the Volcanogenic Massive Sulphides (VMS) types. For this reason, metallogenists have given it a specific name: the Iberian Type (Sáez et al. 1996; Sáez et al. 1999).

The massive sulphides in the IPB are composed mainly of pyrite (all deposits) sometimes with chalcopyrite (*e.g.* Aznalcóllar, El Carmen), sphalerite (*e.g.* Tharsis, San Platón), galena (*e.g.* Los Silos, Neves-Corvo), as well as small quantities of pyrrhotite (*e.g.* Tharsis, Sotiel) (Marcoux et al. 1996). Accessory minerals are described by Marcoux and Leistel (1996).

The gossans in the IPB

In the IPB, two types of sulphide-related iron-oxidized formations can be distinguished: (i) primary or "in place" gossans (true gossans) developed immediately over the sulphide bodies (Filón Sur in Tharsis, La Joya) and (ii) secondary or "remobilized" gossans (false gossans) formed by subsequent supergene weathering, transportation and sedimentation (La Zarza, Alto de la Mesa). To avoid confusion, the latter type of gossan is called a "terrace" (*e.g.* Capitán et al. 2003; Nieto et al., 2003). Wilhelm and Kosakevitch (1978) and Viallefond (1994) show that true gossans generally contain high amounts of Cu, Pb, Ag, As, Sb, Bi, Au and Sn, erratic values in Mo and Co, and low values in Mn, Ni, and B, whereas terraces are rather poor in metals. Several gossans in the IPB have been exploited for gold, such as those at Río Tinto and in the Filón Sur of Tharsis. In the latter gold is enriched up to about ≈ 6 times with an ore content varying between 1 and 3 g/t (Capitán et al. 2003; Nieto et al., 2003). A large number of IPB gossans have been well studied through mineralogical and textural analysis. According to Capitán et al. (2003), the Filón Sur gossan was formed in two main stages: first by oxidation of primary sulphide mineralization above the water table, and second by subsequent weathering. These authors described this gossan as dominated, from bottom to top, by jarosite, goethite and hematite. Hematite is considered to represent the final stage of oxidation.

Method and results

Sampling

Cores were drilled with a portable gasoline drill and oriented using both magnetic and sun compasses when possible to correct local magnetic field anomalies (Tarling and Hrouda, 1993). A total of 214 standard oriented cores were collected from 27 sites with at least 4 samples per site in the RioTinto district of the IPB. Sampling was done of massive sulphides and true gossans at Corta Atalaya, San Miguel, Poderosa and Angostura and from terraces at Alto de la Mesa (Fig. 1c). The gossans and underlying massive pyrite were sampled along vertical profiles to compare the magnetic signals of the primary sulphides and their true gossans. The San Miguel gossan is well developed with massive iron oxide about 15 m thick. Locally the oxides form stalactites in the upper part of the gossan. At Poderosa sampling occurs in a pinched structure very regular from the top of the gossan to the bottom within the massive sulphide zone. In the Angostura pit, samples have been taken in a silicified pinched structure at the top of the gossan and in a massive body in the lower part. At Corta Atalaya, the samples were taken from the stockwork veins and from close to the oxidation front. Finally, the terrace of Alto de la Mesa in Rio Tinto city was sampled in the fine oxihydroxide ribbons where the detrital fraction is low.

Mineralogy of the gossan and massive sulphide

The massive sulphides are mainly composed of pyrite with inclusions of pyrrhotite and chalcopyrite (Fig. 2a and 2b). In the gossans the dominant minerals are iron oxy-hydroxides, mainly goethite and hematite, with ilmenite and quartz (Fig. 2c-2h). Spherulites of goethite crystallized from colloidal solution forms mamillated textures (Figs 2c and 2d). These ribbons

sometimes cover pyrite boxworks or ilmenite. The open spaces between the spherulites are filled by quartz, goethite and hematite fragments. Ilmenite is commonly altered to rutile (Fig. 2g).

Magnetic fabrics study (AMS)

Anisotropy of Magnetic Susceptibility

Magnetic susceptibility (K) is the capacity of a material to be magnetized in a given magnetic field i.e. $K=M/H$ where M and H are the induced and applied magnetic fields, respectively. The susceptibility is described as a symmetric second rank tensor, which can be depicted by an ellipsoid defined by three perpendicularly oriented axes K_1 , K_2 and K_3 (with $K_1 \geq K_2 \geq K_3$). K_1 and K_3 are considered to be the magnetic lineation and the pole of the magnetic foliation, respectively. A number of parameters can be calculated to characterize the AMS ellipsoid, but the most widely used (Tarling and Hrouda 1993) are: the mean magnetic susceptibility (K_m), the anisotropy degree (P'), and the shape parameter (T) with $T > 0$ for an oblate ellipsoid and $T < 0$ for a prolate shape (Jelínek 1978). The definitions of K_m , P' and T are given in Table 1.

Magnetic susceptibility carrier

Magnetic fabrics are usually dominated by ferromagnetic (*s.l.*) phases that have higher magnetic susceptibility and are the main susceptibility carrier(s). Identification of the ferromagnetic phases is necessary to interpret the AMS signal, which has been done using the following techniques: (i) bulk susceptibility measurements (KLY-3S kappabridge apparatus at the Institut des Sciences de la Terre d'Orléans, ISTO), (ii) X-ray diffraction (PW 1380 Philips diffractometer, ISTO), (iii) thermomagnetic experiments (CS3 apparatus coupled with KLY-3S kappabridge, ISTO), (iv) isothermal remanent magnetization (IRM, JR-5A automatic spinner magnetometer, ISTO) and (v) magnetic hysteresis curves (vibrating sample magnetometer (VSM) of Centre Européen de Recherche et d'Enseignement des Géosciences de l'Environnement, (CEREGE, University of Marseilles) and inductometer within an electro-magnet at the Institut de Physique du Globe de Paris (IPGP). The low-temperature magnetism experiments were conducted on a Quantum Design EverCool Magnetic Property Measurement System (MPMS) at the Institut de Physique du Globe de Paris (IPGP).

All studied samples show a positive and high magnetic susceptibility with 95% of having magnetic susceptibilities exceeding 10^{-4} [SI] (Fig. 3) and a clear dominance of ferromagnetic (*s.l.*) minerals with the probable participation of some paramagnetic ones (Rochette et al. 1992; Tarling and Hrouda 1993).

X-ray diffraction was performed on 12 representative samples from different parts of the studied profiles (gossans, terraces and massive sulphides). The gossans are mainly composed of goethite and hematite, while the massive sulphides contain quartz, chlorite and pyrite. It is worth noting that the diffraction spectra of the primary gossans and terraces are similar.

Curie temperature measurements were performed on 11 representative samples. The different paths for heating and cooling, especially in massive sulphides (Fig. 4b), indicate a mineralogical transformation during heating. In the gossans, four susceptibility drops record

Curie temperatures at about 100°C, 300°C, 560°C and 670°C (Fig. 4a). Heating experiments up to 350°C show a cooling curve below the heating path and suggests the destabilization of maghemite. The successive drops could be interpreted as goethite, maghemite destabilization, magnetite (or titanomagnetite) and hematite Curie temperatures (O'Reilly 1984; Dekkers et al. 1989; Dunlop and Özdemir 1997). Some neoformed magnetite and hematite in the gossans appears after heating with the significant increase of the magnetic susceptibility. Therefore, at least some of these results, reflect the transformation of preexisting minerals. In the massive sulphides, a mineralogical transformation is well evidenced by the appearance of magnetite and hematite on the cooling curve (Fig. 4b). During cooling neoformed pyrrhotite has been well defined and probably resulted from the thermal transformation of pyrite. This strong increase of the magnetic susceptibility during cooling at about 300°C is thus due to the abundant formation of hexagonal and monoclinic pyrrhotites. This observation is confirmed by X-ray diffraction measurements carried out on the same samples before and after heating.

Isothermal remanent magnetization (IRM) has been measured for 14 samples of gossan, massive sulphide and terrace samples from different localities. The samples are magnetized in an increasing direct magnetic field and the resulting IRM saturation is characteristic of the different ferromagnetic minerals. The samples from the gossans do not show any magnetic saturation at an applied magnetic field up to 1 Tesla (Fig. 4c), revealing high coercivity magnetic minerals, such as goethite and/or hematite (Dunlop and Özdemir 1997). Samples of massive sulphides show a different behavior i.e. a rapid increase of the induced magnetic moment at weaker applied fields, but without reaching total saturation by 1 T (Fig. 4d). This IRM behavior corresponds to an iron sulphide such as pyrrhotite (O'Reilly 1984).

Hysteresis analysis has been performed on 11 representative samples to test the ferrimagnetic components. The loop from ferromagnetic (*s.l.*) minerals within the gossan (Fig. 4e) is open

and shows clearly the coexistence of ferromagnetic and antiferromagnetic minerals (probably with paramagnetic ones also). This behavior indicates ferromagnetic minerals with a high coercive field (H_c) of 248.8 mT in the gossan. In the massive sulphides, the hysteresis loop shows either a paramagnetic or antiferromagnetic behavior (Fig. 4f). Hysteresis thus suggests the presence of goethite and/or hematite in the gossans, and rather paramagnetic or perhaps hexagonal pyrrhotite within the massive sulphides (Dunlop and Özdemir 1997).

From a magnetic susceptibility point of view, gossans contain goethite and hematite with possibly a trace of magnetite. Though its susceptibility is much weaker than that of magnetite, hematite is probably the principal magnetic fabric carrier because of its great abundance and its high magnetic susceptibility compared to goethite (Rochette et al. 1992). In the massive sulphides, the principal magnetic susceptibility carrier is pyrrhotite in spite of its low abundance.

Selected powdered samples were weighed and subjected to two low temperature magnetism experiments. First, at room temperature (300°K) saturation isothermal remanent magnetization (RT-SIRM) was induced in a 2.5 T field and then its temperature dependence monitored in zero field on cooling from 300°K to 10°K at a $5^\circ\text{K}/\text{min}$ sweep rate. Secondly, at 10°K , the sample was subjected once again to a 2.5 T magnetic field acquiring a low-temperature (LT) SIRM. The temperature dependence of the LT-SIRM was monitored in zero field on warming from 10° to 300°K at a $5^\circ\text{K}/\text{min}$ sweep rate. The latter experiment is analogous to a zero-field cooled (ZFC) experiment after the necessary pre-treatment. The monitoring during cooling will be referenced as RT-SIRM hereafter. The example ZFC curve from a sample of massive sulphide shows a 77% decrease of its initial LT-SIRM by 35°K , then remains constant up to 115°K , and decreases once again by 20% between 115°K and 125°K (Fig. 5a). The initial remanence loss (T_p) is attributed to pyrrhotite as previously

observed by Dekkers (1989) and Rochette et al. (1990). The second remanence loss coincides with the Verwey transition (T_V) of magnetite (Özdemir et al. 1993) where T_V is an electron-ordering transition occurring in a mixed-valent system that results in an ordering of formal valence states in the low-temperature phase. T_V is also observed over the same temperature range on cooling of the RT-SIRM and is equally sharp. Lastly, we observe that only 2% of the ZFC remanence survives thermal demagnetization to 300°K, while 38 % of the RT-SIRM remains following low-temperature demagnetization to 10°K. The sample from gossan (Fig. 5b) does not show any indication of a Verwey transition in either ZFC or RT-SIRM experiments, suggesting the absence of magnetite. It shows a sharp decrease up to 35°K of their ZFC remanence. The amplitude of this decrease is about 30 % of the initial ZFC and much less than the 77 % decrease observed for the massive sulphide sample. Beyond 35°K, the ZFC remanence decreases continuously to a low of 34%. The RT-SIRM increases continuously on cooling such that the remanence at 10°K is 85 % greater than the initial remanence. This low-temperature behavior of the RT-SIRM is reminiscent of goethite (e.g. Guyodo et al. 2006).

Magnetic fabrics

Principal susceptibility axes and other AMS parameters were calculated with the SUSAR program of AGICO. Mean tensors were calculated using Jelínek (1978) statistics; the mean orientations of the principal axes of the ellipsoid of magnetic susceptibility for each site are calculated with "bivariate statistics" (Henry and Le Goff 1995) and the stereograms were plotted using the software Anisoft 4.2 (Chadima and Jelínek 2008).

The AMS data and their associated principal parameters are given in Table 1. In the P' - T plot (anisotropy degree–shape parameter; Fig. 6), the majority of sites display a positive shape parameter, indicating a dominance of magnetic foliation. The degree of anisotropy (P') is mostly lower than 1.02 in the gossans and between 1.02 and 1.05 in the massive sulphides. These low P' values of ≤ 1.05 indicate the absence of deformation in the studied profiles (Tarling and Hrouda 1993).

The results of magnetic fabrics along vertical profiles sampled in the primary gossans and terraces are presented in Figures 7 and 8, respectively. The profile measured from San Miguel (Figs. 7a-7d; 7h-7l and 7s) is the most representative of a primary gossan because it was rooted in massive sulphides and well developed at its top. Along the studied profiles, the general characteristics of magnetic fabrics are as follows. The poles of the magnetic foliation (K_3) give a well-defined average direction. The foliation orientation varies along the profile, being vertical or highly inclined in the massive sulphides (*e.g.* Figs. 7v-7x) and in the lower parts of the primary gossans (*e.g.* Figs. 7l, 7o, 7q and 7t), but horizontal in the upper parts of the primary gossans (*e.g.* Figs. 7a-7e and 7g). Some exceptions to this general trend were observed where the lower part of the gossan had a horizontal foliation (*e.g.* Fig. 7k). These exceptions are probably due to the heterogeneity within the gossans. In terraces, the horizontal magnetic foliation dominates the magnetic fabric (*e.g.* Figs. 8a-8d).

Paleomagnetic study

Thermal demagnetization was applied using a laboratory-built furnace (ISTO). The magnetic remanence was measured using JR5 spinner magnetometer (ISTO) to remove unwanted

modern viscous remanent magnetization components from the magnetic remanence of the specimens. The magnetic remanence directions were isolated by principal component analysis (Kirschvink 1980) and the mean directions were computed by spherical statistics (Fisher 1953) using a paleomagnetic software packages of by Cogné (2003) and R. Enkin (unpublished).

Progressive magnetic remanence cleaning was done in 16 steps from 20 to 700°C. Intensity drops in magnetic remanence intensity-temperature diagrams show the presence of goethite at about 120°C, maghemite (destabilization) at 320°C and a high quantity of hematite at 680°C with rare magnetite at 585°C (Figs. 9a, 9c, 9e and 9g). Figures 9b, 9d, 9f and 9h show representative samples in orthogonal projection on demagnetization (Zijderveld 1967). Two components are usually isolated: a lower temperature component (LTC) from 0 to 150°C, and a higher temperature one (HTC) from about 250 to 680°C that normally decays toward the origin of an orthogonal diagram. The LTC is probably carried by goethite, while the HTC is mainly carried by hematite and pyrrhotite with, sometimes, trace magnetite. The LTCs often exhibit either a normal polarity close to the PEF direction (Figs. 9b, 9d and 9f) or a random direction (Fig. 9h) that probably records the recent geomagnetic field or drilling heating. Nevertheless, the HTCs are stable and differ from the PEF. Both normal (Figs. 9b and 9d) and reversed (Figs. 9f and 9h) polarities for the remanence is indicative of a characteristic remanent magnetization.

As discussed above, the high temperature component is principally carried by hematite and pyrrhotite. The similar magnetic directions recorded by two different minerals indicate that their magnetizations are probably acquired at the same time, at least at a specimen level. Figure 10 presents stereoprojections of magnetic directions obtained from the four primary gossans (Fig. 10a) and the terrace (Fig. 10b). The magnetic directions of each polarity are

well grouped and fit a Fisherian distribution (Fisher 1953). The reversal test of McFadden and McElinny (1990) was applied to each site, and the test is negative for all four gossans, but positive for the terrace (Table 2). In the gossans the reverse polarity is found in the upper part, as is well displayed in the San Miguel gossan where the magnetic fabric foliation is horizontal, and also in the Corta Atalaya oxidised stockwork in the same area with its horizontal foliation. Combining the reversed remanence directions of all gossan samples gives a direction with a declination of 188.2° and an inclination of -55.8° . The normal polarity samples are mainly associated with the lower part of the gossans where the magnetic foliation is partially overprinted, and its declination is 358° and the inclination 51.8° . In the terrace the normal and reversed polarities are mixed and the statistical calculation gives a global mean direction with a declination of 4.1° and an inclination of 62.3° .

Discussion

Magnetic fabrics in gossan from top to bottom

AMS study of several gossan and terrace profiles identifies four different types of magnetic fabrics:

(i) In massive sulphides, the magnetic fabric is characterized by an E–W to NW–SE vertical foliation (*e.g.* Fig. 7v). This foliation is also observed in the country rock shales where two sites also give an E–W magnetic foliation (Fig. 7f) that probably corresponds to a tectonic structure inherited from the Hercynian orogenic phase (*e.g.* Quesada 1998). Although massive

sulphide samples have higher P' values of ≤ 1.05 than the gossans samples of ≤ 1.02 (Fig. 6 and Table 1), these values from the intensely deformed Paleozoic ore deposits are still much lower than those cited for highly deformed rock of >1.2 (Tarling and Hrouda 1993). This suggests either that the massive sulphides have not completely preserved the fabric acquired during deformation, or that they underwent some mineralogical transformations that modified their primary Hercynian deformation fabrics, although the E–W to NW–SE vertical magnetic foliation is still termed a "Hercynian" fabric.

(ii) In the uppermost parts of the primary gossans, the magnetic fabric is characterized by a well-defined horizontal magnetic foliation (*e.g.* Figs. 7a-7e and 7g) with a weak degree of anisotropy (Fig. 6 and Table 1). The horizontality of the magnetic fabric can be explained by compaction of the uppermost zones of the gossan due to leaching of labile elements by meteoric water. This transition between a vertical foliation with relatively stronger P' in sulphide protore to a horizontal foliation with weaker P' in weathered zones is also observed in the lateritic profiles (Mathé et al. 1999; Théveniaut and Freyssinet 1999). This typical fabric is called a "mature" fabric (see below).

(iii) Between the root of massive sulphides and the horizontal fabric at the top of the primary gossans, an intermediate transitional zone can be defined that is a combination of the two fabrics (*e.g.* Figs. 7h-7t). In this zone, the magnetic fabric is characterized by a vertical foliation similar to the massive sulphide fabric but with variable orientations and a very weak anisotropy degree P' , as in the upper parts of the gossans. In this transitional zone, the magnetic response is a mixture of "Hercynian" and "mature" fabric that is termed an "immature" fabric (see below).

(iv) In terraces, the AMS data display a well defined horizontal magnetic foliation (*e.g.* Figs. 8a-8b) that reveals the internal stratification. Such classical "sedimentary fabric" is

extensively described in the AMS literature (Tarling and Hrouda 1993; Charreau et al. 2005). The variation of the anisotropy degree (Fig. 6 and Table 1) probably reflects variable degrees of sediment compaction.

The vertical zonality identified by the magnetic fabrics can be correlated to the mineralogical zoning defined by Capitán et al. (2003) and Nieto et al. (2003) in the Filón Sur of Tharsis gossan where: (i) the upper zones, dominated by hematite, would correspond to their so-called "hematitic gossan"; and, (ii) the lower parts, dominated by goethite and jarosite with scarce hematite, would correspond to their so-called "goethitic and jarositic gossans". The distinction found between the two magnetic fabrics in gossans is also observed in two sites sampled in oxidized stockworks that show the two different fabrics in their corresponding topographic positions. When the stockwork is exposed to intense alteration, it shows a horizontal magnetic foliation (Fig. 7e). Conversely, when it is exposed to a weak alteration, an overprinted magnetic foliation is observed (Fig. 7o).

Capitán et al. (2003) and Nieto et al. (2003) showed that hematite is the typical mineral formed in the last stage of alteration. Thus a fairly good correlation can be drawn between the mineralogical and magnetic fabric zonalities that can be interpreted as the grade of maturation of a gossan. (i) The higher degree of maturation is observed in the upper part of the profile. It is characterized by a higher concentration in hematite, weak values of anisotropy degree (P'), and a horizontal magnetic foliation. The higher maturation grade is defined by a complete obliteration of the fabric inherited from the Hercynian orogeny and the resultant "mature fabric". (ii) The lower degree of maturation is observed in the deeper parts of the gossans. Its main features are (1) the dominance of goethite with respect to hematite, (2) relatively lower values of anisotropy degree P' than in the underlying massive sulphides, and (3) a strongly inclined magnetic foliation that is interpreted to be a relic of the Hercynian orogenic

deformation. The lower maturation grade in the lower part of a gossan corresponds to an "immature fabric".

The boundary between the "Hercynian" and the "immature" fabrics corresponds to an oxidation front (Fig. 12), where the sulphides are oxidized to iron oxi-hydroxides. Also, according to Capitán et al. (2003), Nieto et al. (2003) and this study, the transition zone between "immature" and "mature" fabrics in a gossan corresponds to a dehydration and recrystallization front (Fig. 12).

A scenario of sulphide alteration, formation of the primary gossans and their later development of associated terraces can be proposed as follows. Massive sulphides, initially horizontal (Fig. 12a), were folded during the Hercynian orogeny and acquired an E–W vertical fabric (Fig. 12b). Later, alteration took place and the primary gossans were formed immediately on top of the massive sulphides above the water table. Based upon mineralogical and fabric considerations, two grades of alteration can be distinguished: a higher maturation grade in the upper part of the gossans (Fig. 12c) and a lower maturation grade in the lower part above the massive sulphides (Fig. 12d). The exposed parts of primary gossans may then have undergone chemical weathering and erosion. The fragments of gossan were transported and deposited with iron oxi-hydroxides in the form of terraces, showing a horizontal magnetic foliation (Fig. 12d) and other characteristics of sedimentary environments.

Age of the massive sulphides oxidation and chemical remanent magnetization acquisition

As described above, the high temperature components are principally carried by pyrrhotite and hematite with occasional traces of magnetite. These minerals exhibit a common,

nonpresent Earth field direction as a stable magnetic remanence with both normal and reverse magnetic polarities. Therefore the isolated directions record a characteristic remanent magnetization for the gossans and terraces. To a first order, if the slight angular difference between two polarities of gossans is considered as negligible, two individual paleomagnetic poles are consequently calculated (Table 1): Lat. = 86.6 °, Long. = 157.7°, $\alpha_{95} = 2.2^\circ$ for gossans and Lat. = 83.7 °, Long. = 32.5°, $\alpha_{95} = 6.4^\circ$ for terrace. Figure 10 presents these two paleomagnetic poles from gossans and terrace of this study and all available paleomagnetic data from the Iberian microplate (Schott 1988; Osete et al. 1997). It is obvious that the comparison is almost impossible as the paleomagnetic poles from this microplate are too dispersed (see the details in Schott 1988; Osete et al. 1997). This leads us to compare our newly obtained results with Stable Europe paleopoles as the kinematic history between Iberia and Stable Europe has been well established (e.g. Osete et al. 1997; Rosenbaum et al. 2002; Symons et al. 2009). The comparison with Stable Europe (Besse and Courtillot 2002) can be done directly (Fig. 11a) without any kinematic pre-reconstruction because a Miocene age has been attributed to the gossans by paleontology (Phillips 1881; Moreno et al. 2003), and moreover, the Iberian microplate has been solidly accreted to Stable Europe since 45 Ma (Symons et al. 2009). As only 10 samples were sampled from the terrace, no reliable conclusion could be made though its paleomagnetic pole seems closer to the present Earth's field. It is noteworthy that the positive reversal test may indicate that the terrace deposits may have been formed in a continuous process. The pole of the gossans falls near the 5-15 Ma sector of the apparent polar wander path (APWP) for stable Europe. This first estimate is consistent with previous age estimates (Phillips 1881; Moreno et al. 2003)

Reversal tests on the gossan's remanence directions data reveal a statistically significant negative response. Table 2 lists the paleomagnetic poles of both polarities (Fig. 11b). The slight angular difference between the two gossan poles suggests two distinct periods of

magnetization. Close examination of the polarity distribution along the vertical profiles, suggests a polarity distribution that generally follows the vertical logic of the magnetic fabrics: i.e. the samples carrying the reversed polarity are located in the upper part in the mature part of the gossan and those with normal polarity are in the lower immature part of the gossan except for some mixed polarities in the middle part of the Angostura profile. This vertical polarity distribution accords with the hypothesis that the magnetization has been acquired during two different periods. The paleomagnetic pole of normal polarity is close to the 5-10 Ma sector of the APWP, however, the cone of 95% confidence of the reversed polarity pole intersects the cones of 15-25 Ma poles of the APWP. Although this comparison remains approximate due to the small number of studied samples and probably also to the shorter time of the remanence acquisition, the normal polarity remanence seems to present a younger age than that of the reversed remanence. This observation indicates that the alteration of the massive sulphides took place from top to depth and that the process may involved two main stages.

Two stage alteration of the massive sulphides

Compared to the APWP of Stable Europe (Besse and Courtillot 2002), the ages of the two paleomagnetic poles obtained from this study may correspond to a Late Oligocene to Early Miocene age for the older zones in the upper part of the gossans and a Late Miocene to Early Pliocene age for the younger zones in the lower part of the gossans. This two-stage alteration is probably due to water table changes in response to climatic variation in erosion rates and/or in uplift tectonics.

The first oxidation step occurred in the late Oligocene. This period is marked by large and abrupt climate changes characterized by strong short-term fluctuations of warmer (e.g. the Late Oligocene Warming Event) and colder intervals (e.g. the Oligocene Glacial Maximum)

that have been recognized and correlated around the World (e.g. Zachos et al. 2001; De Man and Van Simaey 2004; Mosbrugger et al. 2005; Alegret et al. 2008). In order to trace the paleoenvironmental evolution across the Oligocene epoch, Alegret et al. (2008) carried out a quantitative analysis of benthonic and planktonic foraminiferal assemblages from the Oligocene section of the Fuente Caldera (Southern Spain). According to these authors, the occurrence of some planktonic foraminiferal species is directly linked to Late Oligocene warming, which induced a major drop in sea level. This event could be the cause of a water table drop that provoked a massive sulphide oxidation (e.g. Alegret et al. 2008).

The second alteration stage in the gossans was probably initiated by a water table drop related to the Messinian Salinity Crisis. The crisis resulted from the drying up of the Mediterranean Sea between 5.96 and 5.33 Ma (Krijgsman 1999), and it is one of the most dramatic Cenozoic climatic events to have occurred on Earth (Hsü 1973). Westward Eocene and Oligocene movement of the Alboran block into the gap between Iberia and northern Africa caused a slab roll-back of Tethys oceanic lithosphere and a closure of the Tethys marine corridor linking the Mediterranean Sea with the Atlantic Ocean (Duggen et al. 2004). Isolation of the Mediterranean Sea resulted in its desiccation in latest Miocene times, causing the Messinian Salinity Crisis (Duggen et al. 2003). The resulting Mediterranean Sea level fall would have caused a water table drop and renewed the alteration of the massive sulphides. Intense erosion has also been inferred to have occurred at this time (Haq et al. 1987; Kosakevitch et al. 1993).

The two-stage alteration identified in the vertical variation of the paleomagnetic signal can be correlated to the AMS observations of this study. The “mature fabric” corresponds to the older age estimated from the reversed magnetic directions and the age of the “immature” lower part of profiles is rather younger. This change in vertical fabric is accompanied by a weak increase in magnetic anisotropy that may be explained by the lower maturation grade of

the alteration. Paleomagnetic and AMS data are coherent with sulphide oxidation and gossan formation in two stages. Besides these geophysical studies based on the rock magnetism, mineralogical investigations of a neighboring gossan (Filón Sur, Tharsis district) reached similar conclusions (Capitán et al. 2003, Nieto et al. 2003). According to these authors, the Tharsis gossan was formed in two main stages; the first stage of which was associated with the oxidation of primary sulphide mineralization above the water table, while the second stage was related to the evolution of the gossan after complete oxidation of the superficial part of the sulphide deposit.

Gossan formation

Sulphide oxidation and evolution of gossans are known to progress from the top (oxidized zone) to the base (protore) with a well distinguished vertical zonation (e.g. Park and MacDiarmid 1964; Jébrak and Marcoux 2008). According to our previous discussion on age the process of gossan formation may be described as follows. The oxidation of pyrite and other sulphides starts to form iron oxi-hydroxides and sulfuric acid. The initial product of weathering is typically an amorphous ferric hydroxide expressed as $\text{Fe}(\text{OH})_3$ that gradually crystallizes to goethite and hematite. Other important minerals associated with the Fe oxides are jarosite, gypsum, clay minerals and silica (e.g. Atapour and Aftabi 2007). The oxidation of the massive sulphides starts at the top and progresses downward to the deeper zones as the oxygenated meteoric waters percolate downward. This process occurred in two main periods, during Late Oligocene to Early Miocene and during Late Miocene to Early Pliocene. AMS fabrics suggest that the transformation in the upper part of a gossan forms an iron cap with a “mature” magnetic fabric similar to a laterite, whereas in their lower part the immature AMS

fabric is younger with a mixed magnetic fabric influenced by Hercynian deformation (Fig. 12c). An alteration phase then evolved in two stages; the first associated with the vertical magnetic foliation and the second with a horizontal foliation (Fig. 12).

The terraces are invariably characterized by a “sedimentary” fabric with mixed magnetic polarities. They may have formed by erosion/alteration, transportation and deposition of primary gossan in a continuous process throughout the two stages of massive sulphide oxidation (Fig. 12).

Conclusions

This study of gossans and their associated massive sulphides in the Spanish section of the Iberian Pyrite Belt (IPB) using Anisotropy of Magnetic Susceptibility (AMS) characterizes the magnetic fabrics in different mineralized settings and distinguishes different maturation grades within a primary gossan. Vertical zoning has been evidenced by three types of magnetic fabrics with intrinsic geological or/and mineralogical characteristics. These magnetic fabrics are: (i) a "Hercynian fabric" found in the massive sulphides and inherited from the Hercynian orogeny (Fig. 12b); (ii) a "mature fabric" observed in the uppermost part of primary gossans, produced by weathering involving meteoric water, and having a higher maturation grade (Fig. 12c); and (iii) an "immature fabric" found between the above two fabrics in the lower part of primary gossans (Fig. 12d). Terraces formed by alteration/erosion, transportation and deposition of gossans are characterized by a "sedimentary" fabric (Fig. 12d). The results of this magnetic investigation agree with those of earlier mineralogical studies (Capitán et al. 2003; Nieto et al. 2003).

As the values for the anisotropy parameter P' are relatively greater in the high maturation zone than in the immature zone, the anisotropy parameter could possibly be an estimate of the grade of maturation in different parts of a primary gossan. Further work is needed to test the reliability of P' as a useful parameter for mapping the grade of maturation and its potential as a mining exploration tool in gossans.

Dating gossans in the Iberian Pyrite Belt reveals a two stages formation. The paleomagnetic signal of gossans is vertically distributed in two zones: (i) a reversed remanence polarity in the upper part and a polarity one in the lower part. Combining this vertical distribution of magnetic polarities with a negative reversal test, it is reasonable to hypothesize that the magnetizations of each polarity were acquired during two distinct periods with an older alteration age at the top and a younger age at the bottom. This observation indicates that the alteration processed from the top of the gossans to depth as for climatic lateritization. These two paleomagnetic dating can be easily correlated to the AMS results. The older age correlates to the horizontal “mature” fabric in the upper part of the gossan and presents a high maturation stage for alteration of the massive sulphides. The younger age correlates to the vertical “immature” fabric in the lower part and indicates a more recent and weaker maturation stage. These two distinct periods may reflect the changes of paleoclimate and/or erosion inducing a water table drop.

Although this comprehensive magnetic study on gossans has proved its efficiency, more detailed work is needed to improve our knowledge of the alteration process in massive sulphides and the formation of gossans. Further studies should focus on the timing relationship between gossans and terraces, and on the possible spatial variation of alteration age with paleoclimatic or local tectonic changes. Moreover, some questions remain that are

more difficult to answer, such as, what was the duration of alteration and magnetization acquisition?

Acknowledgements

We present our thanks to David Symons, Fernando Tornos, Patrick Wiliams and anonymous reviewer for their constructive suggestions to improve the manuscript.

References

- Abad I, Nieto F, Velilla N (2001) The phyllosilicates in diagenetic–metamorphic rocks of the South Portuguese Zone, Southwestern Portugal., *Can Mineralogist* 39: 1571-1589
- Alegret L, Cruz L, Fenero R, Molina E, Ortiz S, Thomas E (2008) Effects of the Oligocene climatic events on the foraminiferal record from Fuente Caldera section (Spain, western Tethys). *Palaeogeogr Palaeoclimatol* 269:94–102
- Al TA, Leybourne MI, Maprani AC, MacQuarrie KT, Dalziel JA, Fox D, Yeats PA (2006) Effects of acid-sulfate weathering and cyanide-containing gold tailings on the transport and fate of mercury and other metals in Gossan Creek: Murray Brook mine, New Brunswick, Canada. *Appl Geochem* 21:1969-1985
- Assiri A, Mousa H (2008) Using ASTER imagery for massive sulphide deposits exploration. *Microwaves, Radar and Remote Sensing Symposium* SBN: 978-1-4244-2688-1:300-303

- Atapour H, Aftabi A (2007) The geochemistry of gossans associated with Sarcheshmeh porphyry copper deposit, Rafsanjan, Kerman, Iran: Implications for exploration and the environment. *J Geochem Explor* 93:47-65
- Besse J, Courtillot V (2002) Apparent and true polar wander and the geometry of the geomagnetic field over the last 200 Myr. *J. Geophys. Res* 107: doi: 10.1029/2000JB000050
- Borradaile GJ, Tarling DH (1981) The influence of deformation mechanisms on magnetic fabrics in weakly deformed rocks. *Tectonophysics* 77:151-168
- Bouillin JP, Bouchez JL, Lespinasse P, Pecher A (1993) Granite emplacement in an extensional setting: an AMS study of the magmatic structures of Monte Capanne (Elba, Italy). *Earth Planet Sci Lett* 118:263-279
- Boyle DR (1995) Geochemistry and genesis of the Murray Brook precious metal gossan deposit, Bathurst Mining Camp, New Brunswick. *Exploration and mining geology* 4:341-363
- Capitán A, Nieto JM, Sáez R, Almodóvar GR (2003) Caracterización textural y mineralógica del gossan del Filón Sur (Tharsis, Huelva). *Boletín de la Sociedad Española de Mineralogía* 26:45-58
- Chadima, M., Jelínek, V. (2008:) Anisoft 4.2. – Anisotropy data browser. In Milan Hvožd'ara (ed) *Paleo, Rock and Environmental Magnetism, 11th Castle Meeting, Contribution to Geophysics and Geodesy, Special issue*. Geophysical Institute of the Slovak Academy of Sciences, Bojnice Castle, Slovak Republic, pp 41
- Charreau J, Chen Y, Gilder S, Dominguez S, Avouac J, Sen S, Sun D, Li Y, Wang W (2005) Magnetostratigraphy and rock magnetism of the Neogene Kuitun He section (northwest China): implications for Late Cenozoic uplift of the Tianshan mountains. *Earth Planet Sci Lett* 230:177-192

- Cogné JP (2003) PaleoMac: A Macintosh™ application for treating paleomagnetic data and making plate reconstructions. *Geochem. Geophys. Geosyst* 4(1) : 1007, doi:10.1029/2001GC000227
- Dekkers, M. J., Mattei, J. L., Fillion, G. & Rochette, P. (1989) Grain-size dependence of the magnetic behavior of pyrrhotite during its low temperature transition at 34 K. *Geophys Res Lett* 16:855–858
- Dekkers MJ (1990) Magnetic monitoring of pyrrhotite alteration during thermal demagnetization. *Geophys Res Lett* 17:779-782
- De Man E, Van Simaëys S (2004) Late Oligocene warming event in the southern North Sea Basin: benthic foraminifera as paleotemperature proxies. *Neth J Geosci* 83: 227–239
- Duggen S, Hoernle K, Van Den Bogaard P, Rüpke L, PhippsMorgan J (2003) Deep roots of the Messinian salinity crisis. *Nature* 422:602–606
- Duggen S, Hoernle K, van den Bogaard P, Harris C (2004) Magmatic evolution of the Alboran region: The role of subduction in forming the western Mediterranean and causing the Messinian Salinity Crisis. *Earth Planet Sci Lett* 218:91–108
- Dunlop DJ, Özdemir Ö (1997) *Rock magnetism : Fundamentals and Frontiers*. Cambridge University Press
- Egal M, Elbaz-Poulichet F, Casiot C, Motelica-Heino M, Négrel P, Bruneel O, Sarmiento A, Nieto J (2008) Iron isotopes in acid mine waters and iron-rich solids from the Tinto-Odiel Basin (Iberian Pyrite Belt, Southwest Spain). *Chem Geol* 253:162-171
- Essalhi M, Sizaret S, Barbanson L, Chen Y, Branquet Y, Panis D, Camps P, Rochette P, Canals A (2009) Track of fluid paleocirculation in dolomite host rock at regional scale by the Anisotropy of Magnetic Susceptibility (AMS): An example from Aptian carbonates of La Florida, Northern Spain. *Earth Planet Sci Lett* 277:501-513

- Evans MA, Lewchuk MT, Elmore RD (2003) Strain partitioning of deformation mechanisms in limestones: examining the relationship of strain and anisotropy of magnetic susceptibility (AMS). *J Struct Geol* 25:1525-1549
- Fisher RA (1953) Dispersion of a sphere. *Proc. Roy. Soc. Lond. A*217: 295–305.3
- González F, Moreno C, Sáez R, Clayton G (2002) Ore genesis age of the Tharsis Mining District (Iberian Pyrite Belt): a palynological approach. *J Geol* 159:229-232
- Guyodo Y, LaPara TM, Anschutz AJ, Penn RL, Banerjee SK, Geiss CE, Zannert W (2006) Rock magnetic, chemical and bacterial community analysis of a modern soil from Nebraska. *Earth Planet Sci Let* 251:168-178.
- Haq BU, Hardenbol J, Vail PR (1987) Chronology of fluctuating sea levels since the Triassic. *Science* 235:1156–1167
- Henry B, Le Goff M (1995) Application de l'extension bivariate de la statistique Fisher aux données d'anisotropie de susceptibilité magnétique: intégration des incertitudes de mesure sur l'orientation des directions principales. *Acad Sc Paris* 320:1037-1042
- Hrouda F (1982) Magnetic anisotropy of rocks and its application in geology and geophysics. *Geophys Surv* 5:37-82
- Hsü KJ, Ryan WBF, Cita MB (1973) Late Miocene desiccation of the Mediterranean. *Nature* 242: 240–244
- Jébrak M, Marcoux E (2008) *Géologie des ressources minérales*. Québec ed. Ministère des ressources naturelles et de la faune, Québec; 667 p
- Jelínek V (1978) Statistical processing of anisotropy of magnetic susceptibility measured on groups of specimens. *Stud Geophys Geod* 22:50–62
- Jover O, Rochette P, Lorand JP, Maeder M, Bouchez JL (1989) Magnetic mineralogy of some granites from the French Massif Central: origin of their low-field susceptibility. *Phys Earth Planet Int* 55:79-92

- Kirschvink J (1980) The least squares line and the analysis of paleomagnetic data. *Geophys J. R Astron Soc* 62: 699–718
- Kosakevitch A (1979) Chapeaux de fer : problème de définition et de nomenclature pratique. *Bulletin du BRGM Section II*:141–149
- Kosakevitch A, García Palomero F, Leca X, Leistel JM, Lenotre N, Sobol F (1993) Contrôles climatique et géomorphologique de la concentration de l'or dans les chapeaux de fer de Río Tinto (Province de Huelva, Espagne). *CR Acad Sci Paris 316–II*: 85-90
- Krijgsman W, Hilgen FJ, Raffi I, Sierro FJ, Wilson DS (1999) Chronology, causes and progression of the Messinian salinity crisis. *Nature* 400: 652–655
- Le Borgne E (1955) Susceptibilité magnétique anormale du sol superficiel. *Ann. Geophys* 11:399–419
- Leblanc M, Morales JA, Borrego J, Elbaz-Poulichet F (2000) 4.500-year-old mining pollution in southwestern Spain: long-term implications for modern mining pollution. *Econ Geol* 95:655–662
- Leistel JM, Marcoux E, Thiéblemont D, Quesada C, Sánchez A, Almodóvar GR, Pascual E, Sáez R (1998c) The volcanic-hosted massive sulphide deposits of the Iberian Pyrite Belt : Review and preface to the Thematic Issue. *Miner Deposita* 33:2-30
- Lécolle M (1972) Successions lithologiques et stratigraphiques dans la Province de Huelva Espagne; position des minéralisations magnésifères et pyriteuses. *CR Acad Sci Paris* 274:505-508
- McFadden PL, McElhinny MW (1990) Classification of the reversal test in Paleomagnetism. *Geophys J Int* 103:725–729

- Marcoux E, Moëlo Y, Leistel JM (1996) Bismuth and cobalt minerals as indicators of stringer zones to massive sulphide deposits, Iberian Pyrite Belt. *Miner Deposita* 31:1-26
- Marcoux E, Leistel JM (1996) Mineralogy and Geochemistry of massive sulphide deposits. Iberian Pyrite Belt. *Boletín Geológico y Minero* 107:3-4
- Mathur R, Ruiz J, Tornos F (1999) Age and sources of the ore at Tharsis and Rio Tinto, Iberian Pyrite Belt, from Re-Os isotopes. *Miner Deposita* 34:790-793
- Mathé P, Rochette P, Vandamme D, Colin F (1999) Volumetric changes in weathered profiles: iso-element mass balance method questioned by magnetic fabric. *Earth Planet Sci Lett* 167:255-267
- Moreno, C (1993) Postvolcanic Paleozoic of the Iberian Pyrite Belt: an example of basin morphologic control on sediment distribution in a turbidite basin. *Jour. Sed. Petrol.*, 63: 1118-1128
- Moreno C, Capitán MA, Doyle M, Nieto JM, F. Ruiz F, Sáez R (2003) Edad mínima del gossan de Las Cruces: Implicaciones sobre la edad del inicio de los ecosistemas extremos en la Faja Pirítica Ibérica. *Geogaceta* 33:67-70
- Moreno, C, Sierra, S, Sáez, R (1996) Evidence for catastrophism at the Famennian–Dinantian boundary in the Iberian Pyrite Belt. In: Strogon, P. Somerville D., Jones, G.Ll. (eds), “Recent Advances in Lower Carboniferous Geology” Geological Society Special Publication, 107:153–62
- Mosbrugger V, Utescher T, Dilcher D (2005) Cenozoic continental climatic evolution of Central Europe. *Proceedings of the National Academy of Sciences (PNAS)* 102: 14964–14969
- Munhá J (1979) Blue amphiboles, metamorphic regime and plate tectonic modelling in the Iberian Pyrite Belt. *Contrib Mineral Petr* 69:279-289

- Munhá J (1990) Metamorphic evolution of the south Portuguese/Pulo do Lobo zone. In Dallmeyer R, Martinez Garcia E (ed) Pre-Mesozoic evolution of Iberia. Berlin, New York, Springer Verlag, pp 363-368
- Nieto JM, Almodóvar GR, Pascual E, Sáez R, Jagoutz E (1999) Estudio isotópico con el sistema Re-Os de las mineralizaciones de sulfuros de la Faja Pirítica Ibérica. *Geogaceta*, 27: 181-184
- Nieto, J.M., Capitán, M.A., Sáez, R., Almodóvar, G.R., 2003. Beudantite: a natural sink for As and Pb in sulphide oxidation processes. *Applied Earth Science (Trans. Inst. Min. Metall. B)*. 112, 293-296.
- Nomade S, Theveniaut H, Chen Y, Pouclet A, Rigollet C (2000) Paleomagnetic study of French Guyana Early Jurassic dolerites: hypothesis of a multistage magmatic event. *Earth Planet Sci Lett* 184:155-168
- O'Reilly, W., 1984. Rock and mineral magnetism. Blackie, Glasgow, 230 p.
- Oliveira JT (1990) South Portuguese Zone: introduction. Stratigraphy and syn-sedimentary tectonism in the South Portuguese Zone. In Dallmeyer RD, Garcia EM (ed) Pre-Mesozoic Geology of Iberia. Berlin, New York, Springer Verlag, pp 333-347
- Onézime J, Charvet J, Faure M, Chauvet A, Panis D (2002) Structural evolution of the southernmost segment of the West European Variscides: the South Portuguese Zone (SW Iberia). *J Struct Geol* 24:451-468
- Osete ML, Rey D, Villalain JJ, Juarez MT (1997) The Late Carboniferous to Late Triassic segment of the apparent polar wander path of Iberia. *Geologie en Mijnbouw* 76: 05–119
- Özdemir Ö, Banerjee S (1982) A preliminary study of soil samples from west-central Minnesota. *Earth Planet Sci Lett* 59:393–403

- Özdemir, Ö., Dunlop, D. J., Moskowitz BM (1993) The effect of oxidation of the Verwey transition in magnetite. *Geophys Res Lett* 20: 1671–1674
- Park CF, MacDiarmid RA (1964) *Ore deposits*. Freeman W.H.
- Phillips JA (1881) Occurrence of remains of recent plants in brown iron ore (Río Tinto). *Q J Geol Soc London* 37:1-5
- Quesada C, Bellido F, Dallmeyer RD, Gil Ibarra I, Oliveira JT, Pérez Estaún A, Ribeiro A, Robardet M, Silva J B (1991) Terranes within the Iberian Massif: correlations with West African sequences. In Dallmeyer R (ed) *The West African Orogens and Circum-Atlantic Correlations*. Berlin, New York, Springer Verlag, pp 267-294
- Quesada C (1998) A reappraisal of the structure of the Spanish segment of the Iberian Pyrite Belt. *Miner Deposita* 33:31-44
- Ribeiro A, Silva JB (1983) Structure of the South Portuguese Zone. In Lemos de Sousa MJ, Oliveira JT (ed) *The Carboniferous of Portugal*. *Memoria Servicos Geológicos de Portugal*, pp 83-89
- Rochette P, Fillion G, Mattéi J, Dekkers MJ (1990) Magnetic transition at 30-34 Kelvin in pyrrhotite: insight into a widespread occurrence of this mineral in rocks. *Earth Planet Sci Lett* 98:319–328
- Rochette P, Jackson M, Aubourg C (1992) Rock magnetism and the interpretation of the anisotropy of magnetic susceptibility. *Rev Geophys* 30:209-226
- Rosenbaum G, Gordon S. L., Duboz D (2002) Relative motions of Africa, Iberia and Europe during Alpine orogeny. *Tectonophysics* 359:117–129
- Routhier P, Aye F, Boyer C, Lecolle M, Moliere P, Picot P, and Roger G (1980) La ceinture sud-iberique à amas sulfurés dans sa partie espagnole médiane. *Mémoire BRGM* 92:265

- Sáez R, Almodovar GR, Pascual E (1996) Geological constraints on massive sulphide genesis in the Iberian Pyrite Belt. *Ore Geol Rev* 11:429-451
- Sáez R, Pascual E, Toscano M, Almodovar GR (1999) The Iberian type of volcano-sedimentary massive sulphide deposits. *Miner Deposita* 34:549-570
- Sáez, R., Nocete, F., Nieto, J.M., Capitán, M.A., Rovira, S. (2003) The extractive metallurgy of copper from Cabezo Juré, Huelva, Spain: Chemical and mineralogical study of slags dated to the Third Millenium B.C. *Can. Mineralogist* 41:627-638
- Sáez R, Moreno C, González F (2008) Synchronous deposition of massive sulphide deposits in the Iberian Pyrite Belt: New data from Las Herrerías and La Torerera ore-bodies. *Comptes Rendus Geosciences* 340:829-839
- Schermerhorn LJG, Stanton WI (1969) Folded overthrusts at Aljustrel. *Geological Magazine* 106:130-141
- Schermerhorn LJG (1971) An outline stratigraphy of the Iberian Pyrite Belt. *Boletín Geológico y Minero* 82:238-268
- Schott JJ, Peres A (1988) Palaeomagnetism of Permo-Triassic red beds in the western Pyrenees: evidence for strong clockwise rotations of the Palaeozoic unit. *Tectonophysics* 156: 75–88
- Scott KM, Ashley PM, Lawie DC (2001) The geochemistry, mineralogy and maturity of gossans derived from volcanogenic Zn-Pb-Cu deposits of the eastern Lachlan Fold Belt, NSW, Australia. *J Geochem Explor* 72:169-191
- Silva J, Oliveira J, Ribeiro A (1990) Structural outline of the south Portuguese zone. In Dallmeyer R, Martinez, García, E. (ed) *Pre-Mesozoic Geology of Iberia*. Berlin, New York, Springer Verlag, pp 348-362
- Sizaret S, Chen Y, Marcoux E, Touray J-C, (2001) Anisotropie de susceptibilité magnétique (ASM) et chimie des traces : une nouvelle méthodologie pour démêler processus

hydrothermaux et supergènes. Application au gisement à Ba-Fe-F de Chaillac (Indre, France). CR Acad Sci Paris, Earth and Planetary Sciences, 332:431-437

Sizaret S, Chen Y, Chauvet A, Marcoux E, Touray JC (2003) Magnetic fabrics and fluid flow directions in hydrothermal systems. A case study in the Chaillac Ba-F-Fe deposits (France). Earth Planet Sci Lett 206:555-570

Sizaret S, Chen Y, Barbanson L, Camps P, Henry B, Marcoux E (2006). Crystallisation in flow Part I: paleo-circulation track by texture analysis and magnetic fabrics. Geophys J Int, 167:605-612

Sizaret S, Fedioun I, Barbanson L, Chen Y (2006b) Crystallisation in flow Part II: Modelling crystal growth kinetics controlled by boundary layer thickness. Geophys J Int 167:1027-1034

Sizaret S, Branquet Y, Gloaguen E, Chauvet A, Barbanson L, Arbaret L, Chen Y (2009) Estimating the local paleo-fluid flow velocity: New textural method and application to metasomatism. Earth Planet Sci Lett 280:71-82

Soriano C (1996) Tectonica del cabalgamientos en la Faja Piritica Iberica (Zona Sur Portuguesa): la lamina de cabalgamiento de Sanlucar de Guadiana y el antiformal de Puebla de Guzman. Geogaceta 20:786-788

Symons DTA, Lewchuk MT, Boyle DR (1996) Pliocene–Pleistocene genesis for the Murray Brook and Heath Steele Au–Ag gossan ore deposits, New Brunswick, from paleomagnetism. Can J Earth Sci 33(1):1–11

Symons DT, Lewchuk MT, Kawasaki K, Velasco F, Leach DL (2009) Dating of the Reocin MVT Deposit, Spain, by Paleomagnetism. Miner Deposita 44:867-880

Talbot JY, Faure M, Chen Y, Martelet G (2005) Pull-apart emplacement of the Margeride granitic complex (French Massif Central). Implications for the late evolution of the Variscan orogen. J. Struct. Geol 27:1610-1629

Tarling, D.H., Hrouda, F., 1993. *The Magnetic Anisotropy of Rocks*. Chapman and Hall, London, 217 p.

Théveniaut H, Freyssinet P (1999) Paleomagnetism applied to lateritic profiles to assess saprolite and duricrust formation processes: the example of Mont Baduel profile (French Guiana). *Palaeogeogr Palaeoclim* 148:209-231

Tornos F (2006) Environment of formation and styles of volcanogenic massive sulphides: The Iberian Pyrite Belt. *Ore Geology Reviews* 28:259-307

Van den Boogaard MV (1963) Conodonts of the Upper Devonian and Lower Carboniferous age from Southern Portugal. *Geologie en Mijnbouw* 42:248-259

Viallefond L (1994) Cluster analysis on geochemical results from gossans. In Leistel JM, Bonijoly D, Braux C, Freyssinet P, Kosakevitch A, Leca X, Lescuyer JL, Marcoux E, Milési JP, Piantone P, Sobol F, Tegye M, Thiéblemont D, Viallefond L (ed) *The massive sulphide deposits of the South Iberian Pyrite Province: geological setting and exploration criteria*. BRGM, France, pp 109-229

Wilhelm E, Kosakevitch A (1978) Chapeaux de fer. Rapport BRGM "Valorisation des ressources du sous-sol" 78SGN710MGA:

Wilhelm E, Kosakevitch A (1979) Utilisation des chapeaux de fer comme guide de prospection. *Bulletin du BRGM section II*:109–140

Zachos J, Pagani M, Sloan L, Thomas E, Billups K (2001) Trends, rhythms, and aberrations in global climate 65 Ma to present. *Science* 292:686–693

Zijderveld JDA (1967) A.C. demagnetization of rocks: Analysis of results. In Collinson DW, Creer KM, Runcorn SK (ed) *Methods in paleomagnetism*, pp 254–286

Figure captions:

Figure 1. a. Simplified geological map of the major structural units and tectonostratigraphic domains in the South Portuguese Zone and locations of the major volcanogenic massive sulphide deposits of the Iberian Pyrite Belt (after Quesada et al., 1991); Aj: Aljustrel, Az: Aznalcóllar, CP: Campofrío Pluton, Hr: Herrerías, IPB: Iberian Pyrite Belt, NC: Neves–Corvo, PG: Puebla de Guzmán anticline, PQ: Phyllite–Quartzite Group, RT: Río Tinto (the Alto de la Mesa terrace is located in the RT district), Th: Tharsis, VSC: Volcano-Sedimentary Complex, Za: La Zarza. b. Stratigraphic column of the Iberian Pyrite Belt (after Tornos, 2006). c. Detailed map showing the sampling localities. An: Angostura, CA: Corta Atalaya, Po: Poderosa, SM: San Miguel, Th: Tharsis, Za: La Zarza.

Figure 2. Textures of massive sulphides (a-b) and associated gossans (c-h): bo: boxwork, cpy: chalcopyrite, go: goethite, gel: colloidal gel, he: hematite, il: ilmenite, po: pyrrhotite, pore: porosity, py: pyrite, qz: quartz.

Figure 3. Interval of bulk magnetic susceptibility of all measured specimens.

Figure 4. Magnetic mineral analyses of representative samples from a gossan (left) and a massive sulphide (right). a and b: thermomagnetic measurements. Horizontal arrows show the evolution of the heating and cooling stages, whereas the vertical ones show different Curie temperatures and the associated minerals; go: goethite, he: hematite, m-he: maghemite, mg: magnetite and po: pyrrhotite; c and d: isothermal remanent magnetization measurements; e and f: hysteresis curves after correction for the

paramagnetic contribution. The inset diagram of e and f shows the noncorrected measurements.

Figure 5. RT-SIRM cooling branch (filled circles) and ZFC (open circles) curves for (a) a massive sulphide, and (b) a gossan sample. Horizontal arrows indicate the temperature heating and cooling stages, and vertical arrows show the transition temperatures. Tv: Verwey transition, go : goethite, po : pyrrhotite.

Figure 6. Graphic presentation of the shape parameter T versus the corrected anisotropy degree P' for all sites. PG: primary gossans, MS: massive sulphides, OS: oxidized stockworks, SR: surrounding rocks, Te: terraces.

Figure 7. Stereographic projections in lower hemisphere of AMS responses from the San Miguel, Corta Atalaya, Poderosa and Angostura mines. The stereograms are presented along a relative vertical profiles, from the upper part (a to f) and lower part (g to t) of the gossans and the massive sulphides (u to y) profiles. Mean orientations of the principal axes were calculated with bivariate statistics (Henry and Le Goff 1995). ■, ▲ and ● correspond to K_1 , K_2 and K_3 , respectively. Magnetic foliation is defined by the K_1 – K_2 plane, and the magnetic lineation corresponds to the K_1 axis. Ellipses around poles correspond to the interval of confidence at the 95% level. Lithology of sites is given in Table 1.

Figure 8. Magnetic fabric measured in the terrace located at Alto de la Mesa in Rio Tinto city; ■, ▲ and ● are K_1 , K_2 and K_3 , respectively.

Figure 9. Relative remanent magnetization intensity vs. temperature (left) and orthogonal projection in geographic coordinates (right) for progressive thermal demagnetization of representative samples (Zijderveld 1967). Filled and open symbols represent horizontal and vertical planes respectively. Vertical arrows show the Curie (Néel) temperatures; go: goethite; he: hematite; mg: magnetite; m-he: maghemite.

Figure 10. Equal-area projection of specimen remanence directions in stratigraphic coordinates for gossans (a) and terrace (b). Stars represent the averages of normal and reversed polarities of each field.

Figure 11. Paleomagnetic poles calculated from: all gossan samples (star), normal-polarity samples of gossan (large solid circle), reversed-polarity samples of gossan (large open circle) directions of gossans and mean direction of terrace (cross), with: (a) all available paleomagnetic data for the Iberian microplate (a; Schott 1988; Osete et al. 1997), and (b) the 20 and 30 paleopoles of Stable Europe (b; Besse and Courtillot 2002).

Figure 12. Sketch of the evolution of the Iberian pyrite belt gossans from their deposition until the setting of sedimentary terraces with the associated magnetic fabrics and ages given by paleomagnetic studies. DF: dehydration front, MW: meteoric water; N: north; OF: oxidation front; Sw: Stockworks; WT: water table. Small and large circles represent the AMS fabrics and the vertical distribution of the magnetic remanence normal (filled symbols) and reversed (open symbols) polarities, respectively).

Table captions

Table 1. AMS data and associated parameters from this study. PG: primary gossan, MS: massive sulphides, OS: oxidized stockworks, SR: surrounding rocks, Te: terrace, n: number of measured samples, P': corrected anisotropy degree, T: shape parameter (T>0 for oblate shape, and T<0 for prolate ones, Jelínek 1978), K_m : bulk magnetic susceptibility, $K_m = (K_1 + K_2 + K_3)/3$, D: declination, I: inclination, K_1 , K_2 , and K_3 : the axes of the maximum, intermediate and minimum of the ellipsoid of magnetic

susceptibility, respectively. $P' = \exp \left[2 \sum_{i=1}^3 \left(\ln(K_i / K_{moy}) \right)^2 \right]^{\frac{1}{2}}$,

$T = [2(\ln K_2 - \ln K_3) / (\ln K_1 - \ln K_3)] - 1$ (Jelinek, 1978).

Table 2. Mean paleomagnetic directions and corresponding poles for studied gossans and terrace of the Río Tinto District; n: number of samples; Dec.: declination; Inc.: inclination; k: precision parameter; α_{95} : 95% confidence circle around the mean direction (pole); $P_{Lat.}$ and $P_{Lon.}$: latitude and longitude of pole, respectively, calculated at 37.72°N and 6.64°E.

Values with star (*) are not retained for our interpretation, and double star (**) are calculations requiring more samples to be reliable.

Figures

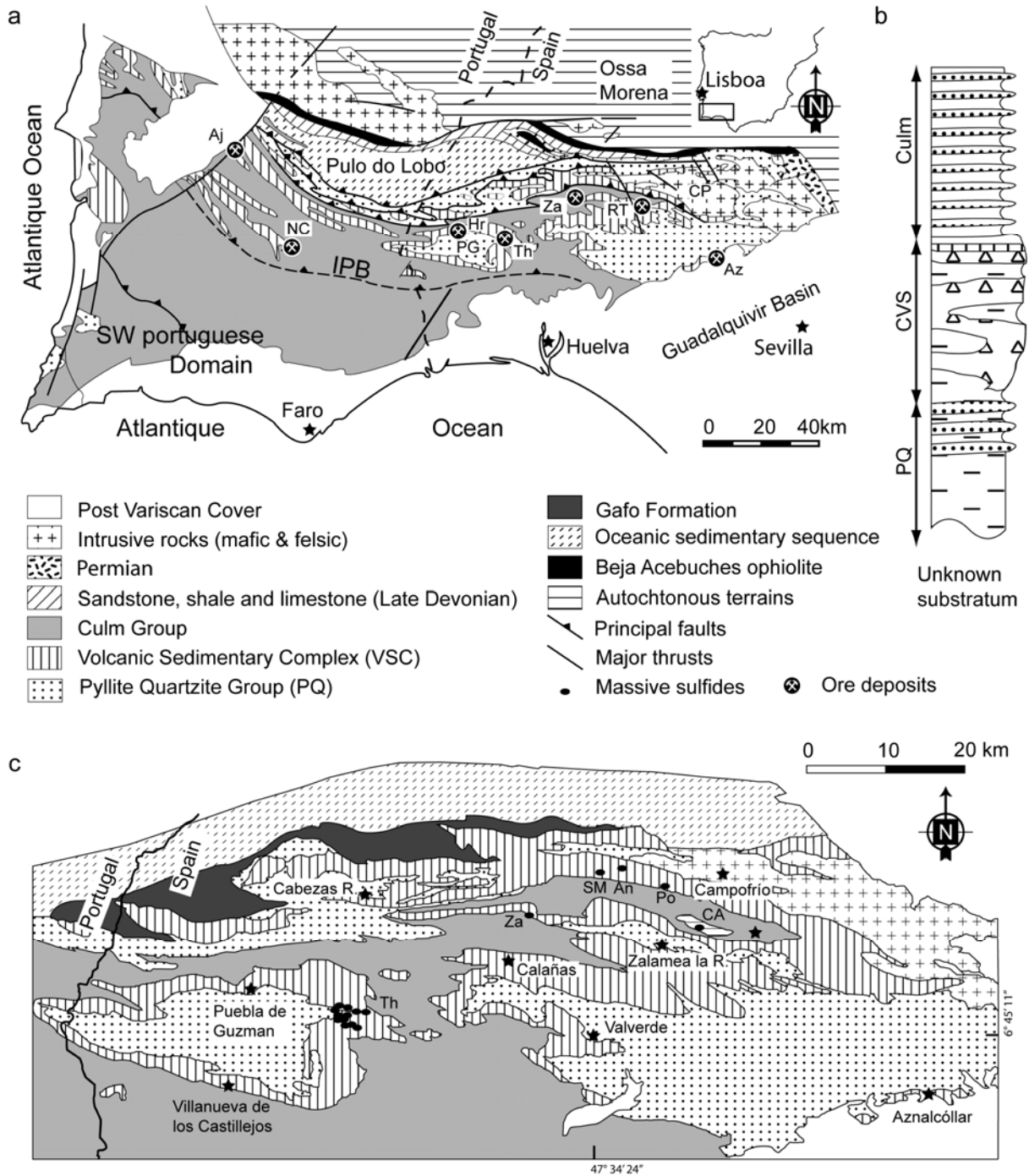


Figure 1. a. Simplified geological map of the major structural units and tectonostratigraphic domains in the South Portuguese Zone and locations of the major volcanogenic massive sulfide deposits of the Iberian Pyrite Belt (after Quesada et al., 1991); Aj: Aljustrel, Az: Aznalcóllar, CP: Campofrío Pluton, Hr: Herrerías, IPB: Iberian Pyrite Belt, NC: Neves-Corvo, PG: Puebla de Guzmán anticline, PQ: Phyllite–Quartzite Group, RT: Río Tinto (the Alto de la Mesa terrace is located in the RT district), Th: Tharsis, VSC: Volcano-Sedimentary

Complex, Za: La Zarza. b. Stratigraphic column of the Iberian Pyrite Belt (after Tornos, 2006). c. Detailed map showing the sampling localities. An: Angostura, CA: Corta Atalaya, Po: Poderosa, SM: San Miguel, Th: Tharsis, Za: La Zarza.

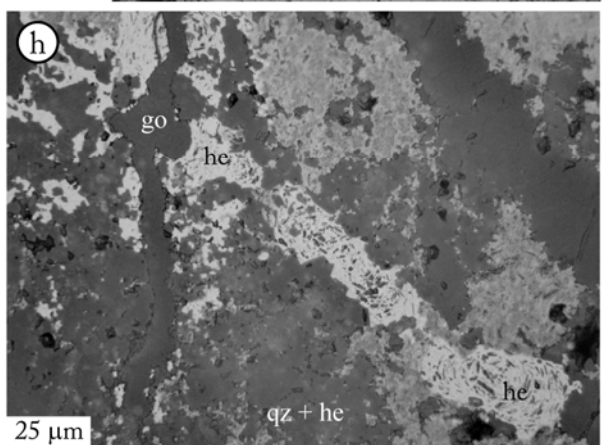
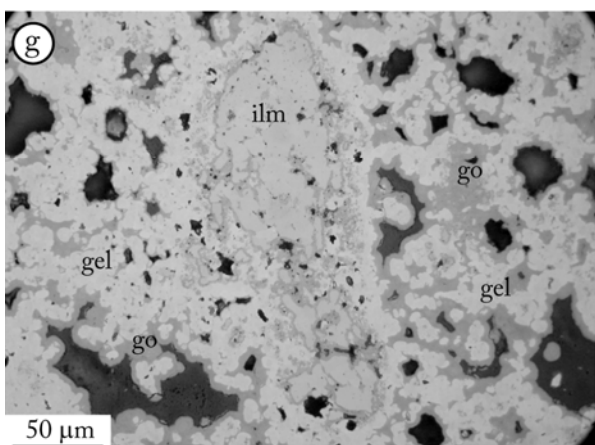
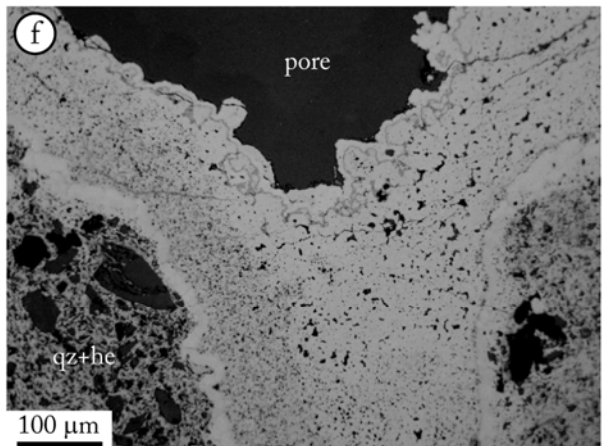
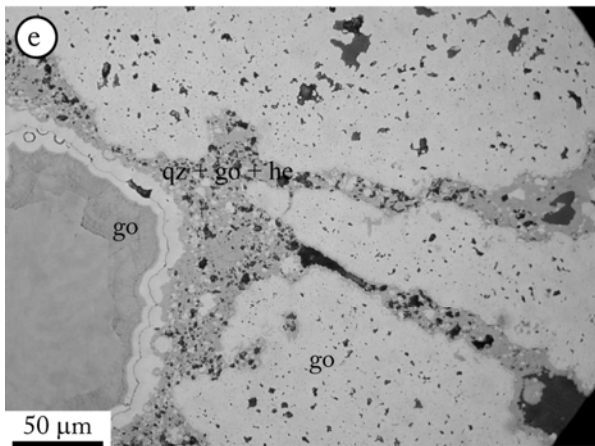
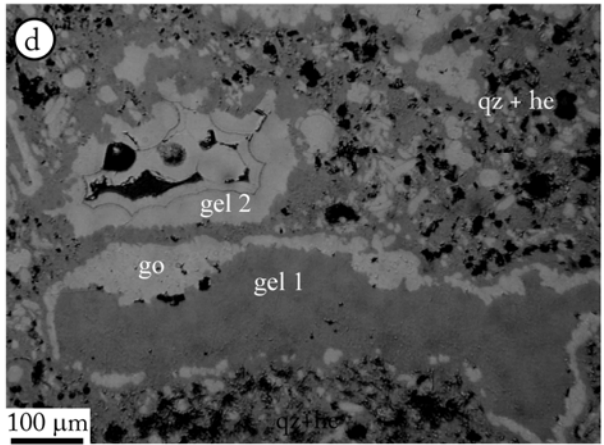
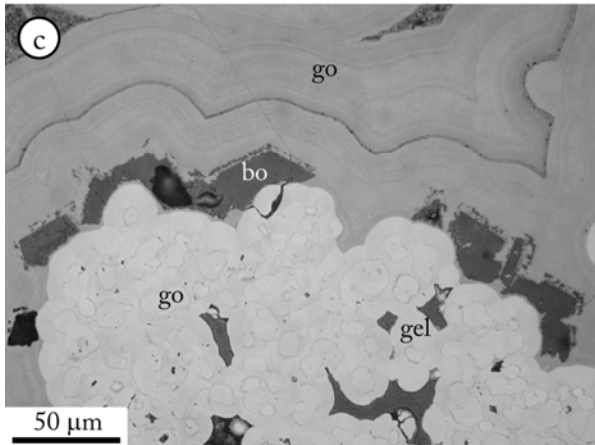
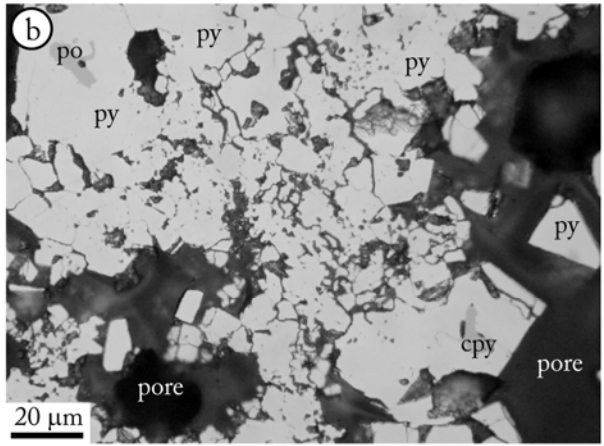
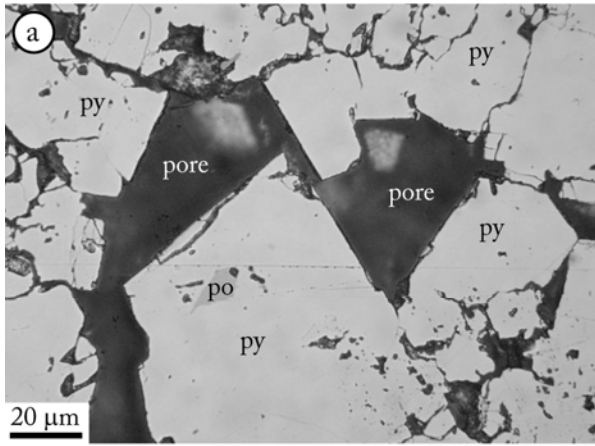


Figure 2. Textures of massive sulfides (a-b) and associated gossans (c-h): bo: boxwork, cpy: chalcopyrite, go: goethite, gel: colloidal gel, he: hematite, il: ilmenite, po: pyrrhotite, pore: porosity, py: pyrite, qz: quartz.

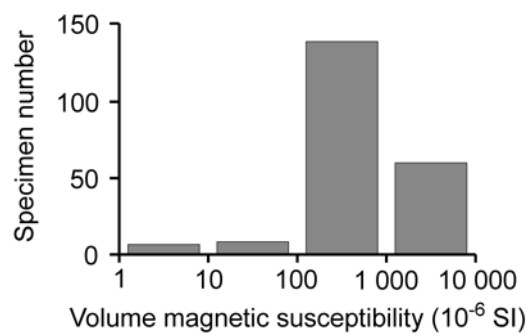


Figure 3. Interval of bulk magnetic susceptibility of all measured specimens.

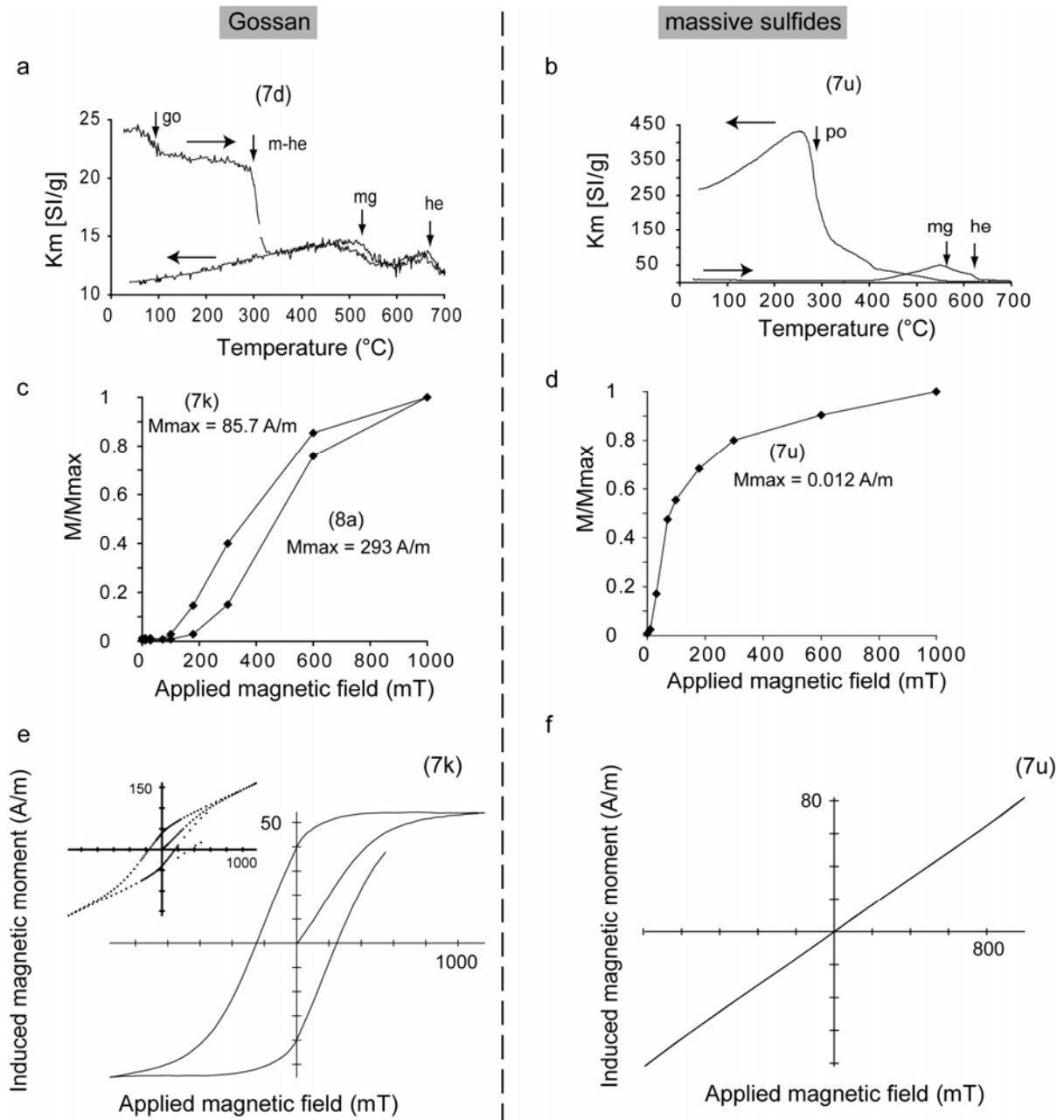


Figure 4. Magnetic mineral analyses of representative samples from a gossan (left) and a massive sulfide (right). a and b: thermomagnetic measurements. Horizontal arrows show the evolution of the heating and cooling stages, whereas the vertical ones show different Curie temperatures and the associated minerals; go: goethite, he: hematite, mg: magnetite and m-he: maghemite; c and d: isothermal remanent magnetization measurements; e and f: hysteresis curves after correction for the paramagnetic contribution. The inset diagram of e and f shows the noncorrected measurements.

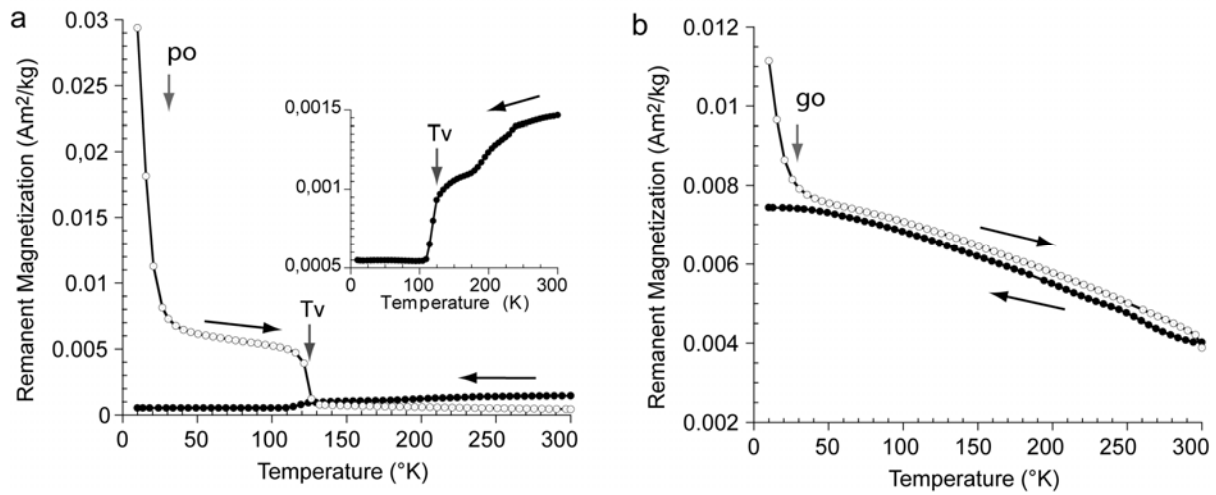


Figure 5. RT-SIRM cooling branch (filled circles) and ZFC (open circles) curves for (a) a massive sulfide, and (b) a gossan sample. Horizontal arrows indicate the temperature heating and cooling stages, and vertical arrows show the transition temperatures. Tv: Verwey transition, go : goethite, po : pyrrhotite.

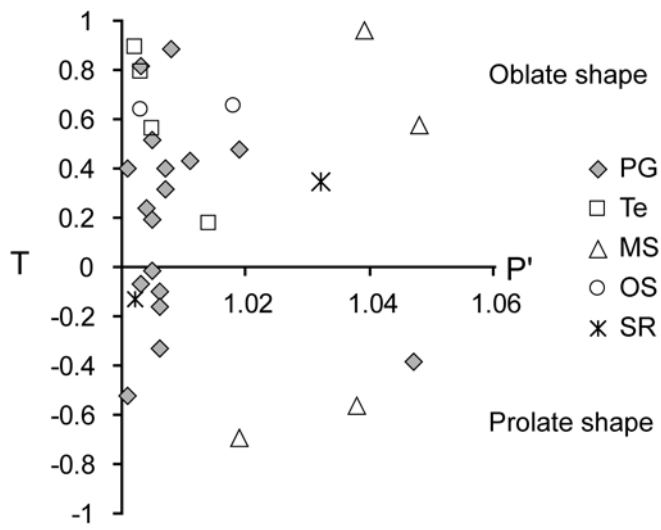


Figure 6. Graphic presentation of the shape parameter T versus the corrected anisotropy degree P' for all sites. PG: primary gossans, MS: massive sulfides, OS: oxidized stockworks, SR: surrounding rocks, Te: terraces.

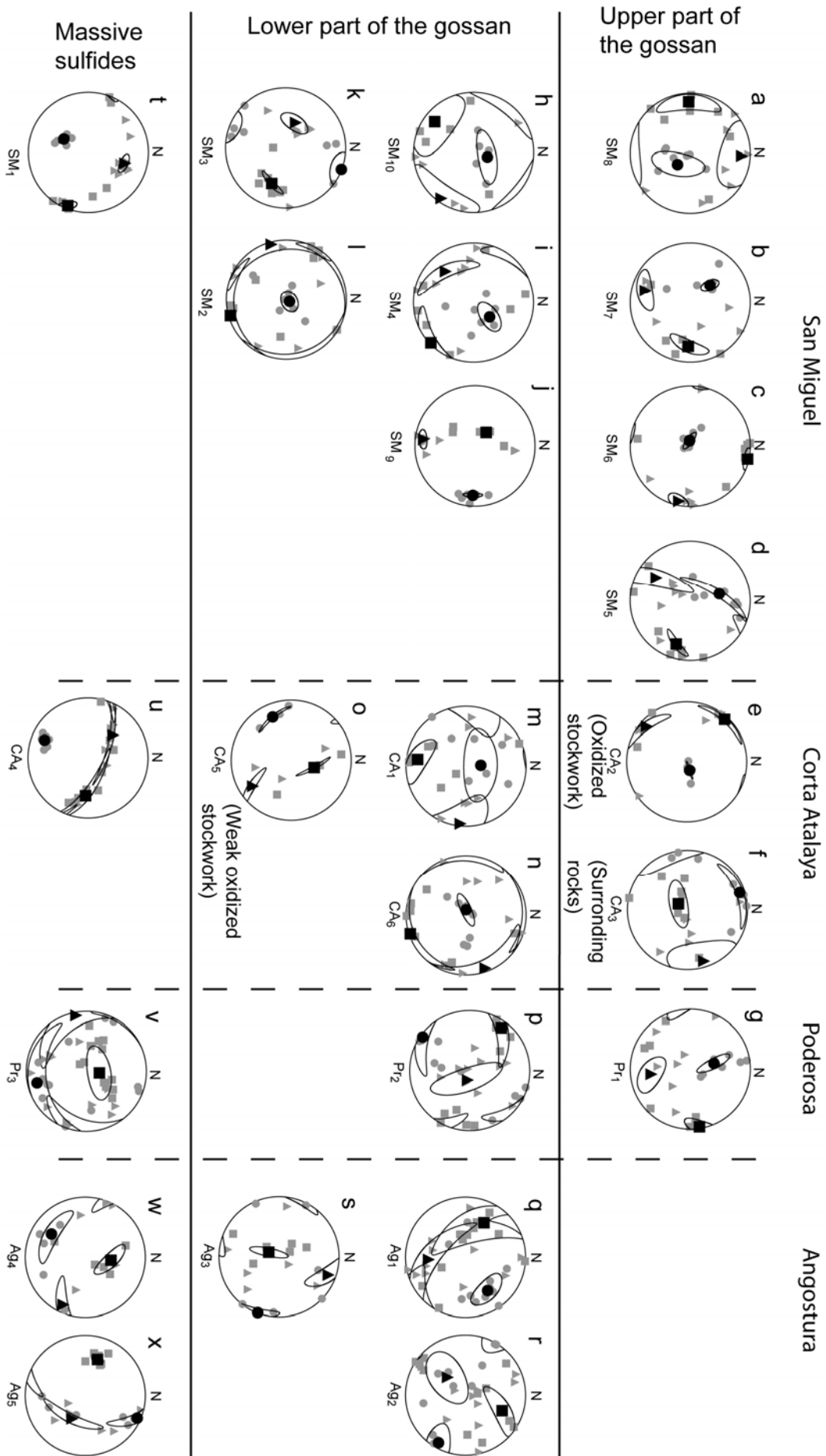


Figure 7. Stereographic projections in lower hemisphere of AMS responses from the San Miguel, Corta Atalaya, Poderosa and Angostura mines. The stereograms are presented along a relative vertical profiles, from the upper part (a to f) and lower part (g to t) of the gossans and the massive sulfides (u to y) profiles. Mean orientations of the principal axes were calculated with bivariate statistics (Henry and Le Goff 1995). ■, ▲ and ● correspond to K_1 , K_2 and K_3 , respectively. Magnetic foliation is defined by the K_1 – K_2 plane, and the magnetic lineation corresponds to the K_1 axis. Ellipses around poles correspond to the interval of confidence at the 95% level. Lithology of sites is given in Table 1.

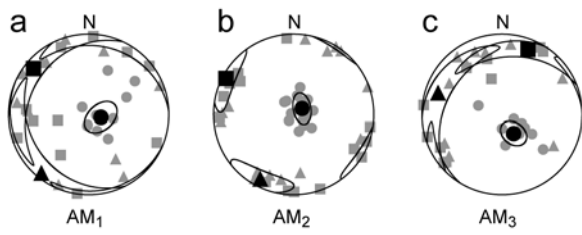


Figure 8. Magnetic fabric measured in the terrace located at Alto de la Mesa in Rio Tinto city;

■, ▲ and ● are K_1 , K_2 and K_3 , respectively.

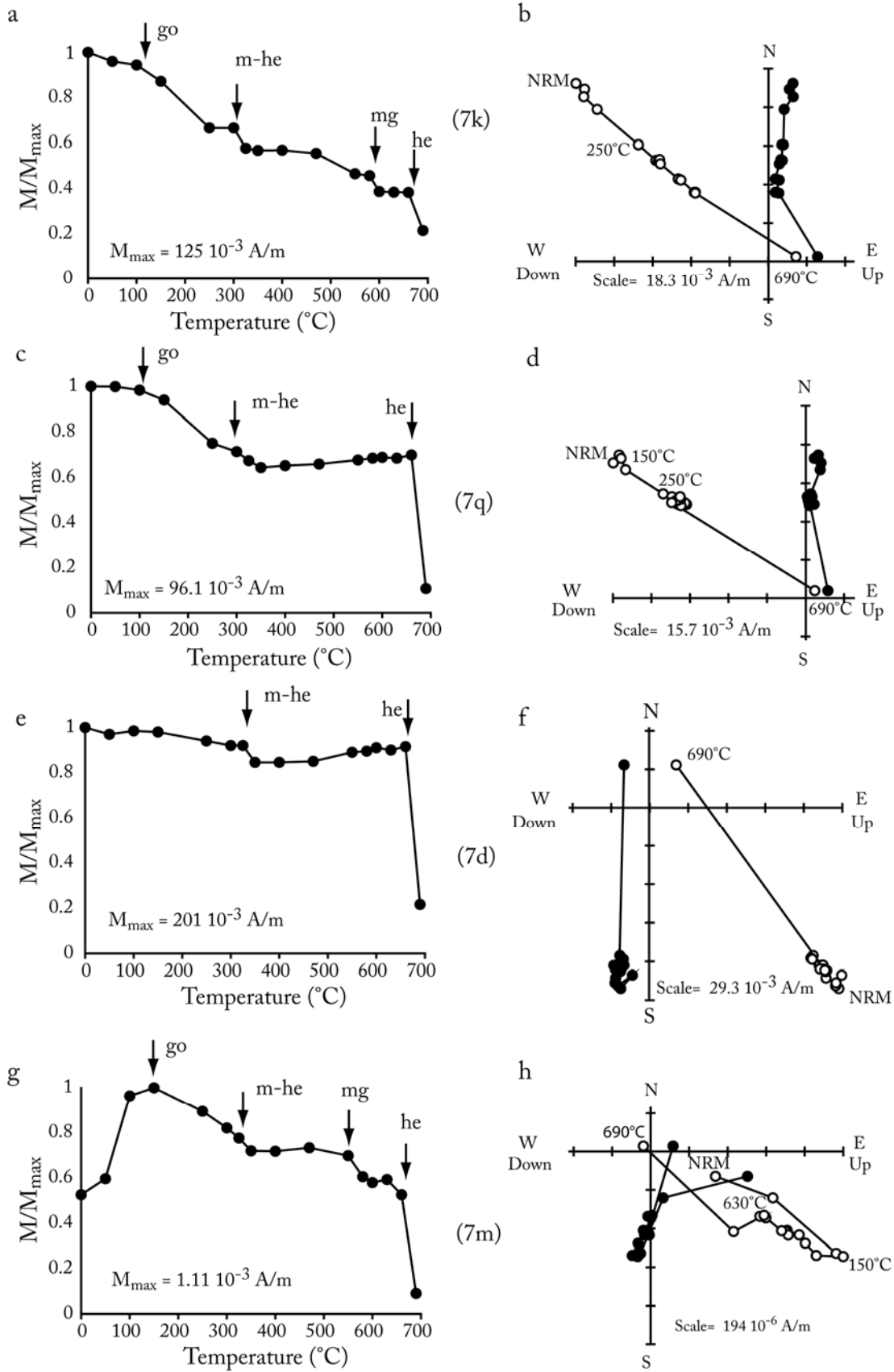


Figure 9. Relative remanent magnetization intensity vs. temperature (left) and orthogonal projection in geographic coordinates (right) for progressive thermal demagnetization of

representative samples (Zijderveld 1967). Filled and open symbols represent horizontal and vertical planes respectively. Vertical arrows show the Curie (Néel) temperatures; go: goethite; he: hematite; mg: magnetite; m-he: maghemite.

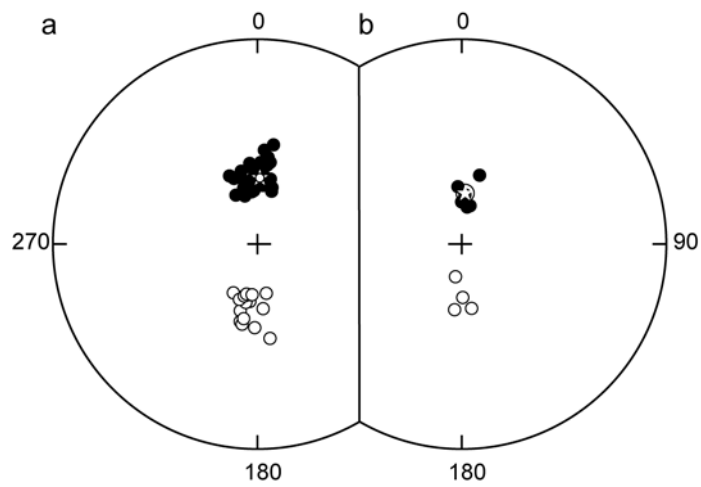


Figure 10. Equal-area projection of specimen remanence directions in stratigraphic coordinates for gossans (a) and terrace (b). Stars present the averages of normal and reversed polarities of each field.

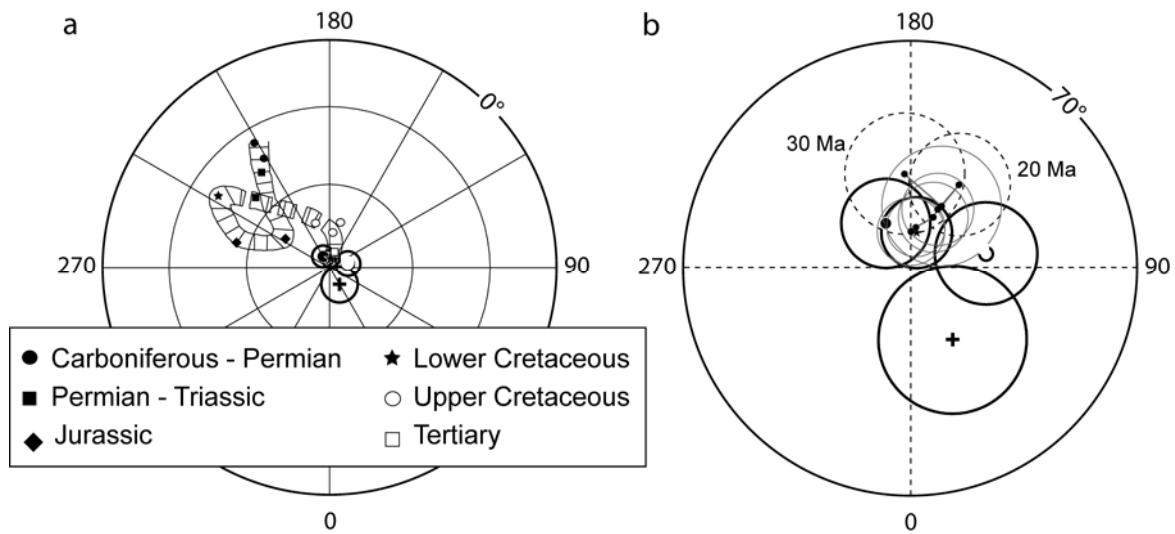


Figure 11. Paleomagnetic poles calculated from: all gossan samples (star), normal-polarity samples of gossan (large solid circle), reversed-polarity samples of gossan (large open circle) directions of gossans and mean direction of terrace (cross), with: (a) all available paleomagnetic data for the Iberian microplate (a; Schott 1988; Osete et al. 1997), and (b) the 20 and 30 paleopoles of Stable Europe (b; Besse and Courtillot 2002).

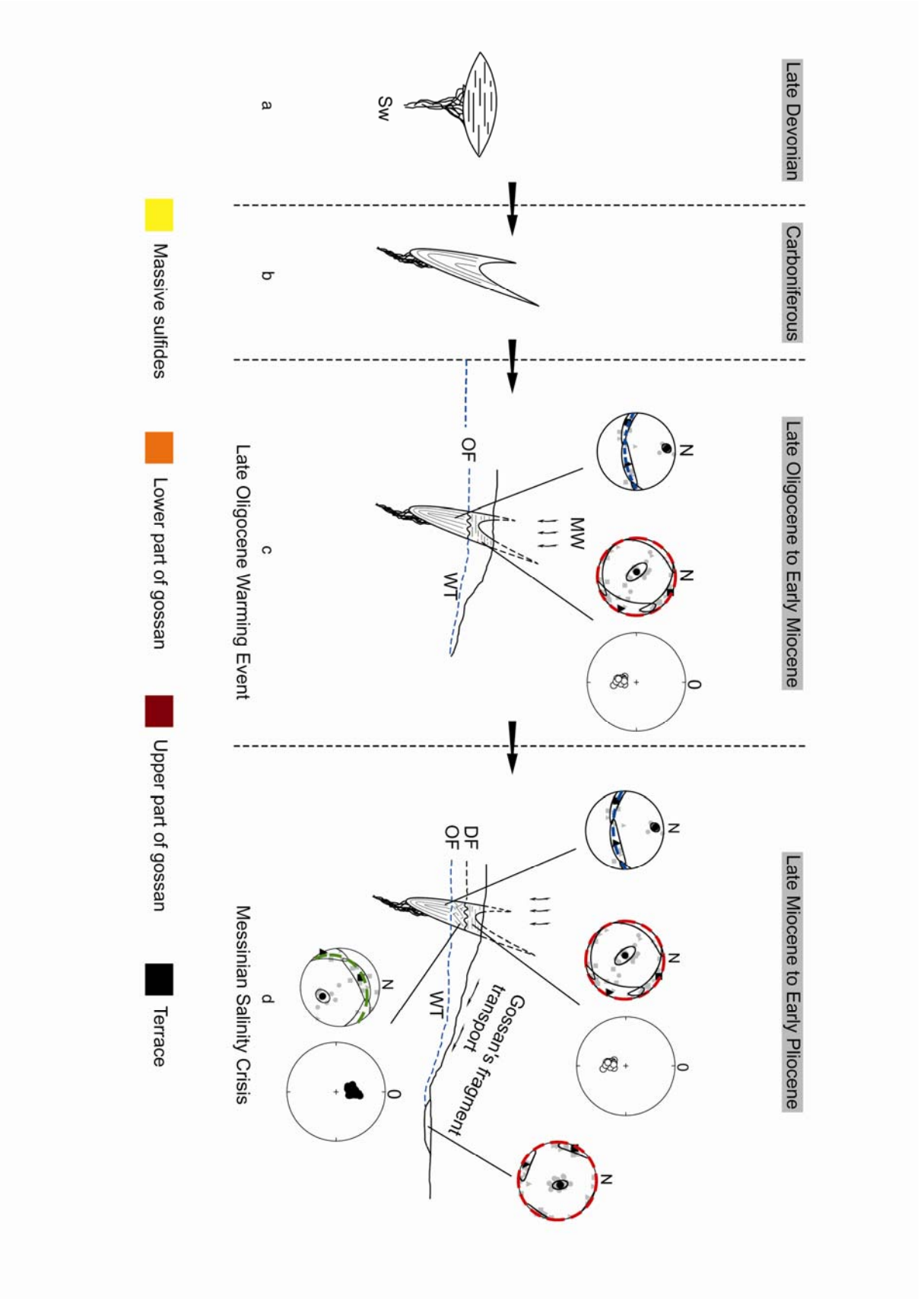


Figure 12. Sketch of the evolution of the Iberian pyrite belt gossans from their deposition until the setting of sedimentary terraces with the associated magnetic fabrics and ages given by paleomagnetic studies. DF: dehydration front, MW: meteoric water; N: north; OF: oxidation front; Sw: Stockworks; WT: water table. Small and large circles represent the AMS fabrics and the vertical distribution of the magnetic remanence normal (filled symbols) and reversed (open symbols) (reversed) polarities, respectively).

Table captions

Depth	Fig.	n	Kv	P'	T	K1	K2	K3				
(m)			x10 ⁻⁶ [SI]			D (°)	I (°)	D (°)	I (°)	D (°)	I (°)	
San Miguel (Gossan), 37°45'42", 6°44'58"												
PG	3	7a	7	1820	1,019	0.475	268.3	15.3	3	16.9	138.5	66.9
PG	3.5	7b	6	699	1.005	0.515	92.6	27.2	194.6	22.2	318.3	53.7
PG	4	7c	8	1290	1.007	0.398	12.3	2.4	102.6	7.3	263.8	82.3
PG	6	7d	8	1210	1.006	-0.102	107.8	24.7	213.7	30.8	346.4	48.7
PG	7	7h	5	596	1.007	0.314	218.1	18.6	126.1	6.1	18.7	70.3
PG	8	7i	7	1660	1.011	0.432	136.3	2.2	227.5	29.7	42.4	60.2
PG	9	7j	7	549	1.047	-0.383	310.1	66.4	187.2	13.3	92.5	19.1
PG	12	7k	7	1100	1.006	-0.331	111.4	36.7	290.1	53.3	21	0.6
PG	14	7l	8	457	1.003	0.815	163.7	3.3	254	3.9	33.6	84.9
MS	16	7t	9	362	1.048	0.575	111.2	5.6	16.9	37.8	208.3	51.7
Corta Atalaya (Gossan) 37°42'12", 6°35'51"												
PG	10	7m	7	5960	1.001	-0.526	188.2	19.7	96.7	4	355.8	69.9
PG	10.2	7n	8	374	1.001	0.398	161.5	2.3	71.2	7	269.5	82.6
MS	10.7	7o	9	986	1.039	0.958	93.7	37.3	316.4	44	202.4	22.8
OS	11.4	7u	3	124	1.018	0.653	17.2	57.1	146.8	22.4	246.8	22.8
OS		7e	4	355	1.003	0.635	311.8	5.9	220.7	10.4	70.8	78
SR		7f	7	872	1.002	-0.128	213.3	75.6	73.5	11.3	341.6	9.2
Poderosa (Gossan) 37°44'55", 6°39'13"												
PG	3	7g	7	7050	1.006	-0.161	81	3.1	173	33.2	346.6	56.6
PG	3.5	7p	10	465	1.005	0.189	306.5	12.5	107.8	76.8	215.6	4.1
MS	4	7v	12	13	1.038	-0.561	6.3	72.2	258.6	5.6	166.9	16.8
Angostura (Gossan) 37°46'01", 6°43'11"												
PG	3	7q	11	439	1.003	-0.069	22.9	34.2	223.3	54.1	119.6	9.7
PG	5	7r	11	530	1.008	0.881	298.1	35.3	176.4	36.6	56.5	33.8
PG	9	7s	6	407	1.004	0.237	203.4	74.8	20.8	15.2	110.9	0.7
PG	13	7w	5	433	1.005	-0.016	6.9	54.6	116	13.1	214.5	32.2

MS	14	7x	6	925	1.019	-0.695	288.7	36.7	121.8	52.5	23.5	6.3
----	----	----	---	-----	-------	--------	-------	------	-------	------	------	-----

Alto de la Messa (Gossan) 37°44'55", 6°39'13"

Te	0.3	8a	11	1200	1.002	0.894	309.5	11.5	218.4	5.5	103.4	77.2
Te	1.3	8b	15	963	1.005	0.559	297.8	4.8	207.1	9.1	55.6	79.7
Te	2	8c	10	1200	1.003	0.792	21.8	14.1	287.3	17.4	148.6	67.3

Table 1. AMS data and associated parameters from this study. PG: primary gossan, MS: massive sulfides, OS: oxidized stockworks, SR: surrounding rocks, Te: terrace, n: number of measured samples, P': corrected anisotropy degree, T: shape parameter (T>0 for oblate shape, and T<0 for prolate ones, Jelínek 1978), K_m : bulk magnetic susceptibility, $K_m = (K_1 + K_2 + K_3)/3$, D: declination, I: inclination, K_1 , K_2 , and K_3 : the axes of the maximum, intermediate and minimum of the ellipsoid of magnetic susceptibility,

respectively. $P' = \exp \left[2 \sum_{i=1}^3 \left(\ln(K_i / K_{moy}) \right)^2 \right]^{\frac{1}{2}}$, $T = [2(\ln K_2 - \ln K_3) / (\ln K_1 - \ln K_3)] - 1$ (Jelinek, 1978).

Zone	n	Dec. (°)	Inc. (°)	k	α_{95} (°)	PLat. (°N)	PLon. (°E)	α_{95} (°)
San Miguel (Gossan)	22*	2.4	49.2	34.7	5.2	83.1	167.5	4.9
N	12	359.5	44.7	28.6	8.3	79.6	190.1	7.0
R	10	186.5	-54.5	71.7	5.7	84.0	115.0	6.3
Corta Atalaya (Gossan)	9*	7.7	53.4	122.1	4.7	82.6	122.9	5.8
N	4	0.4	50.2	377.6	4.7	83.3	182.7	5.8
R	5	194.2	-55.6	162.1	6.0	78.5	199.0	7.1
Poderosa (Gossan)	6	9.3	57.5	415.4	3.3	82.5	90.7	4.3
Angostura (Gossan)	18*	352.7	55.9	47.7	5.1	84.3	275.9	5.9
N	16	352.1	55.2	44.8	5.6	83.5	269.0	6.4
R	2**	180.1	-62.2	146.8	20.8	83.8	6.9	32.6
Alto de la Mesa (Terrace)	9	4.1	62.3	102.1	5.1	82.7	30.8	6.5
N	5*	7.0	63.6	113.8	7.2	80.5	36.1	9.7
R	4*	180.8	-60.6	80.4	10.3	85.3	17.2	13.5
All Gossan	55*	1.0	53.2	43.7	2.9	86.8	169.5	3.1
Normal polarity	38	358.0	51.8	38.8	3.8	85.5	208.1	8.9
Reversed polarity	17	188.2	-55.8	84.7	3.9	83.2	101.0	4.5

Table 2. Mean paleomagnetic directions and corresponding poles for studied gossans and terrace of the Río Tinto District; n: number of samples; Dec.: declination; Inc.: inclination; k: precision parameter; α_{95} : 95% confidence circle around the mean direction (pole); P_{Lat.} and P_{Lon.}: latitude and longitude of pole, respectively, calculated at 37.72°N and 6.64°E.

Values with star (*) are not retained for our interpretation, and double star (**) are calculations requiring more samples to be reliable.